Investigation of Cryolite Ratio Measurement by Potentiometric Methods

A thesis presented in partial fulfilment of

the requirements for the degree of

Masters of Technology in Chemical Technology

at Massey University, Palmerston North,

New Zealand.

Aaron Marshall

2002

Abstract

The cryolite ratio of an industrial aluminium electrolyte can effect many variables within the process including the overall energy efficiency. Careful control of the cryolite ratio is therefore very important. Currently no online measurements of the cryolite ratio are used in industry.

The use of potential measurements between a sodium alloy electrode and an aluminium electrode, as a means of cryolite ratio measurement was investigated. The observed potential changes during cryolite ratio step changes were typically of the correct direction and of similar magnitude to the predicted potential changes calculated from activity data.

The cryolite ratio of the electrolyte was found to change continuously during experiments. This was mainly due to the evaporation of $NaAlF_4$, which was identified by X-ray diffraction. This change in the cryolite ratio meant that long term stability of the electrodes was difficult to accurately quantify.

Electrode damage was found to occur after several hours of use and was contributed to the intrusion of electrolyte into the porous boron nitride used as the electrode body. Furthermore the activity of the sodium alloy electrode was found to change significantly during experiments due to the loss of sodium into the electrolyte. This damage to the electrodes is thought to have effected the stability of measurements considerably.

Dropping metal electrodes were investigated as a possible means of overcoming the changes in electrode activity. The overall stability of the potential measured between a dropping Pb-Na electrode and an aluminium electrode was somewhat better than the stability of potentials measured between two static pool electrodes. Operating difficulties with the dropping Pb-Na electrode combined with the short lifetime of these electrodes makes these electrodes unsuitable for industrial use.

Some suggestions have been made for future electrode designs with single use designs recommended as the most viable option especially for industrial use.

Acknowledgements

I would firstly like to thank the relevant people for the following scholarships, which without I would not been able to carry out this work.

- Dick and Mary Earle Scholarship for Technology
- Masters Scholarship (Massey University)
- Massey Scholarship

I would also like to thank my supervisor Dr Richard Haverkamp, who first got me interested in this field and provided a lot of assistance during the project.

I also thank my parents who encouraged my scientific interests and supported me during my undergraduate degree and of course Sonia who has endured my interests and scientific babblings and provided constant love and support.

Aaron Marshall
February 2002

Table of Contents

List of Figures

List of Tables

1 Introduction & Literature Review

1.1 Introduction to the aluminium industry

1.1.1 Aluminium Production

Aluminium is produced by the electrochemical reduction of alumina (Al_2O_3) as shown by Equation 1.1.

$$2Al_2O_3 + 3C \rightarrow 4Al + 3CO_2 \qquad (1.1)$$

This reaction is performed industrially in the Hall-Héroult cell, named after Hall and Héroult who independently developed the current method of smelting aluminium in 1886. Figure 1.1 shows a schematic of the Hall-Héroult cell.

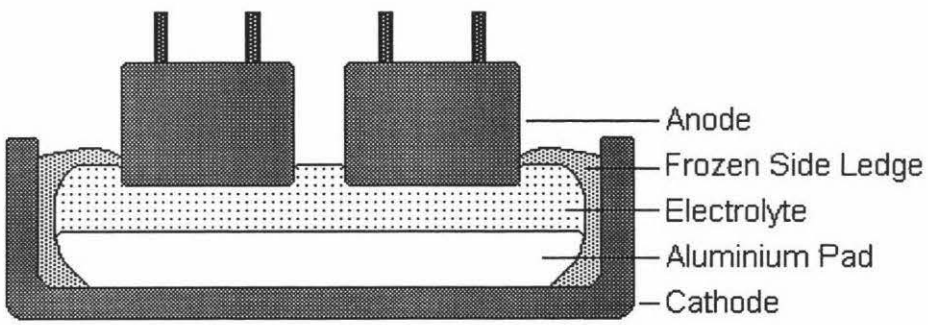

Figure 1.1 Hall-Héroult Cell Schematic

Total annual production of aluminium is reaching close to 24 million tonnes per year [1].

1.1.2 The Hall-Héroult Cell

The Hall-Héroult cell consists of 4 main components, the anode, cathode, aluminium pad, and electrolyte.

The anode is made from a mixture of petroleum coke and coal pitch, and provides the carbon for the reaction, as shown in Equation 1.1. Anodes can either be classified as Prebake or Söderberg anodes depending on their construction method. As the name suggests Prebake anodes are baked into a carbonaceous block before being placed into the cell. Söderberg anodes are baked in position, using waste heat from the cell. The anodes have conducting rods inserted into them, which provides the electrical current to drive the electrochemical reaction. The reaction oxidises carbon from the anode, which means the anodes must be continually lowered into the electrolyte or renewed to maintain the electrical contact with electrolyte.

Like the anode, the cathode is constructed from petroleum coke and coal pitch, also having steel conductor bars inserted through it to carry the electrical current from the cell. The cathode is not used up in the reaction, so it is only replaced once the high temperatures and corrosive electrolyte damage it. Because of the highly corrosive nature of the electrolyte a frozen ledge of electrolyte is allowed to form on the sides of the cathode to reduce the wear and damage.

The aluminium pad is simply the molten aluminium, which is produced during the process. The level of this liquid pad will increase continuously as the aluminium is produced. This means that the aluminium must be siphoned out by vacuum once the level exceeds a set height. Failure to remove the aluminium can result in the anode touching the aluminium pad causing short circuits. Some aluminium should always be present to minimise the wear of the carbon cathode from the corrosive electrolyte.

The electrolyte is where the reaction to reduce alumina takes place. The electrolyte should have the following characteristics to be successful for smelting aluminium.

- High alumina solubility
- Low aluminium solubility
- High electrical conduction
- Low raw material cost
- Higher decomposition voltage than alumina

Currently, only cryolite (Na_3AlF_6) based electrolytes are used for industrial aluminium electrolysis. Further detail on the electrolyte will be given in the following sections.

1.2 Electrolyte Composition

1.2.1 Industrial Electrolytes

As mentioned in the previous section the electrolyte is made up principally of cryolite (Na_3AlF_6). Most industrial smelter cells operate with the addition of aluminium fluoride (AlF_3), as well as calcium fluoride (CaF_2), and occasionally magnesium fluoride (MgF_2), sodium chloride (NaCl), and lithium fluoride (LiF) to improve cell performance. The electrolyte will also contain dissolved alumina (Al_2O_3) that undergoes reduction to produce aluminium.

1.2.2 Cryolite and Bath Ratio

The cryolite ratio (CR) is used to describe the composition of the electrolyte within the smelter cell. It is defined as the molar ratio of sodium fluoride to aluminium fluoride. For pure cryolite the cryolite ratio is equal to 3.

$$CR = \frac{\text{moles NaF}}{\text{moles } AlF_3} \tag{1.2}$$

Another term that is often used, is the bath ratio (BR). This is simply the mass ratio of sodium fluoride to aluminium fluoride. Due to the molecular masses of sodium fluoride and aluminium fluoride, the bath ratio is approximately half the cryolite ratio.

$$BR = \frac{\text{mass NaF}}{\text{mass } AlF_3} \approx \frac{1}{2} CR \tag{1.3}$$

Because most cells operate with additions of AlF_3, excess AlF_3 weight percentages are often quoted.

1.2.3 Typical Composition of an Industrial Electrolyte

Typically, an industrial electrolyte consists of cryolite, 5-15 wt% AlF_3 [2,3], 2-5 wt% Al_2O_3 [2,3], and 3-8 wt% CaF_2 [3]. This corresponds to a cryolite ratio of approximately 2.1-2.65. Other additives, such as MgF_2, LiF, and NaCl [4] have also been used in industrial electrolytes

1.3 Effect of Electrolyte Composition on Smelter Cell Variables

The aim of this section is to show how the electrolyte composition can affect many important variables within an aluminium smelter cell. Due to the nature of this work the emphasis will be placed on how the cryolite ratio or excess AlF_3 concentration affects these variables.

As aluminium production has relatively low energy efficiency, the goal should be to maximise the overall energy efficiency of the process by careful selection and control of the electrolyte composition. This discussion will also consider how each variable can affect the energy efficiency of the overall process. It should be noted that many of the variables within a smelter cell are highly correlated and it is often difficult to accurately determine the effect of a single variable.

1.3.1 Liquidus, Superheat, and Bath Temperature

Due to the high temperatures used during aluminium smelting, this variable should be examined to some degree. There are three temperatures within a smelter cell that can be considered: Liquidus, Bath, and Superheat Temperature.

The liquidus temperature is simply the temperature at which the electrolyte melts. As Figure 1.2 shows, there is considerable variance in the liquidus temperature over the NaF-AlF_3 system. Typical industrial electrolytes have liquidus temperatures ranging from 930 to 985 °C (based on 1.2.3 and [5]).

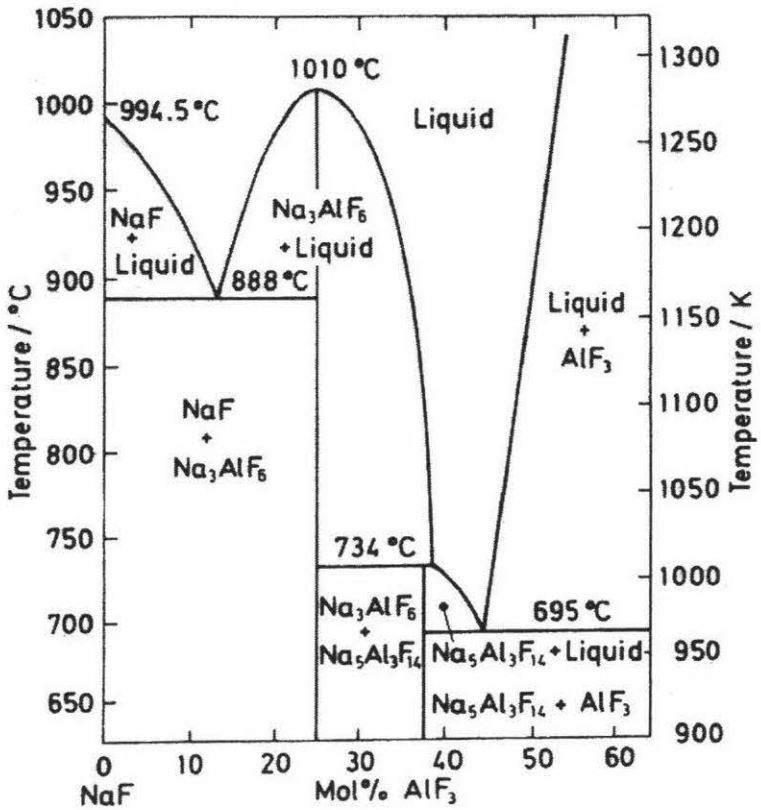

Figure 1.2 NaF-AlF_3 Phase Diagram [6]

The bath temperature is the actual temperature of the electolyte within the cell and is a result of the bath composition and thermal balance of the cell [7]. The bath temperature must be above the liquidus temperature for the electrolyte to be in a liquid state. The superheat temperature is the difference between the bath and liquidus temperatures. The superheat of the electrolyte is important when considering the thermal balance and therefore the side ledge of the cell [2,7-9].

Temperature of the bath has been shown to affect many other variables within the cell such as electrical conductivity [10], density of aluminium and electrolyte [11], and alumina dissolution rate [12,13]. It has also been shown that decreasing the cryolite ratio to lower the liquidus and bath temperatures, results in an increase of the current efficiency [14,15].

1.3.2 Alumina Solubility and Dissolution Rate

As the goal of the Hall-Héroult process is to produce aluminium, alumina must be dissolved into the electrolyte to enable the reaction shown by Equation 1.1 to proceed. This indicates that alumina solubility and dissolution rate are important variables when operating a smelter cell. It has been shown that the composition of the bath is an important factor in the dissolution rate of alumina [12,13] and alumina solubility [16]. Temperature has also been found to affect the dissolution rate of alumina [12,13]. Maintaining and controlling the dissolved alumina concentration is also important in reducing the occurrence of anode effects in the cell [17], which are characterised by rapid increases in the cell voltage and emission of greenhouse gases such as CF_4 and C_2F_6.

1.3.3 Aluminium Solubility and Re-oxidation

One disadvantage of cryolite based electrolytes, is the solubility of aluminium metal. The loss of aluminium by dissolution and then re-oxidation in the electrolyte melt corresponds to a significant loss in the current efficiency [4] (see 1.3.7). The re-oxidation of dissolved aluminium can occur via the following reactions (referred to as back reactions).

$$2Al + 3CO_2 \rightarrow Al_2O_3 + 2CO \qquad (1.4)$$

$$2Al + 3CO \rightarrow Al_2O_3 + 2C \qquad (1.5)$$

It has been shown that the cryolite ratio and the temperature [18] can affect the solubility of aluminium, and ultimately the current efficiency.

Equation 1.6 shows a correlation for the aluminium solubility as a function of bath composition and temperature [19].

$$DM = -0.288 + 0.0003\,t + 0.027\,BR - 0.0019[CaF_2] - 0.0036[LiF] - 0.0029[NaCl] \quad (1.6)$$

where: concentrations e.g. $[CaF_2]$ are in wt%

BR = Bath ratio

T = Temperature (°C)

DM =Dissolved Aluminium concentration (wt%)

1.3.4 Heat Balance and Side Ledge

The heat balance of the cell is a very important factor when both designing and operating a Hall-Héroult cell. Because of the highly corrosive nature of the cryolite based electrolyte a frozen side ledge must be formed to protect the side lining of the cell. This frozen side ledge is formed when the electrolyte temperature at the sides is below the liquidus temperature causing the electrolyte to solidify. This side ledge is rich in cryolite (CR = 3) so changes in the size of the side ledge effects the bulk composition of the bath. The heat balance of the cell (i.e. the balance between the heat loss and heat gain) affects the size of this side ledge.

To illustrate the effect which bath composition has on the side ledge and heat balance, the effect of an AlF_3 addition can be examined [7]. Upon an AlF_3 addition, the liquidus temperature of the electrolyte decreases. This will result in the superheat of the bath increasing, as initially the bath temperature will not decrease. This increase in superheat will cause some of the side ledge to be re-melted, resulting in the cryolite ratio of the electrolyte being higher than expected after the AlF_3 addition. The smaller side ledge will allow higher heat loss through the side lining eventually lowering the bath temperature and reforming more side ledge. During this change in the cells heat balance there will also be a number of other variable changes such as electrical resistance, aluminium solubility, density, and of course current and energy efficiency [7]. If the heat balance of the cell is not managed correctly, cell failure can arise from corrosion and thermal damage of the side lining.

1.3.5 Electrical Conductivity

As the reduction of alumina to aluminium is carried out electrochemically, the electrical conduction of the cell is very important in minimising the total electricity consumption. There has been much work carried out in this area with some very comprehensive reviews available [20]. The widely accepted Choudhary model for the electrical conductivity of cryolite-based electrolytes was developed over 25 years ago [21] (Equation 1.7).

$$\ln\kappa = 2.0156 - 0.0207[Al_2O_3] - 0.005[CaF_2] - 0.0166[MgF_2] + 0.0178[LiF] + 0.0063[NaCl] + 0.2175CR - \frac{2068.4}{T} \quad (1.7)$$

where: concentrations e.g. $[Al_2O_3]$ are in wt%

CR = cryolite ratio

T = Temperature (K)

κ =electrical conductivity ($S.cm^{-1}$)

There have been other models suggested [22], which also show that the cryolite ratio and concentration of other additives effect the electrical conductivity of the electrolyte.

1.3.6 Density

The density is a vital factor that can affect the performance of the Hall-Héroult cell [11]. The density of NaF_3-AlF_3 melts is shown at various temperatures (Figure 1.3).

The difference in density between the electrolyte and the aluminium pad has a major effect on the stability of the bath-metal interface [11]. At fixed bath compositions, the density difference increases with increasing temperature [11]. Bath composition also contributes to the density induced flow patterns found close to the side ledge [11].

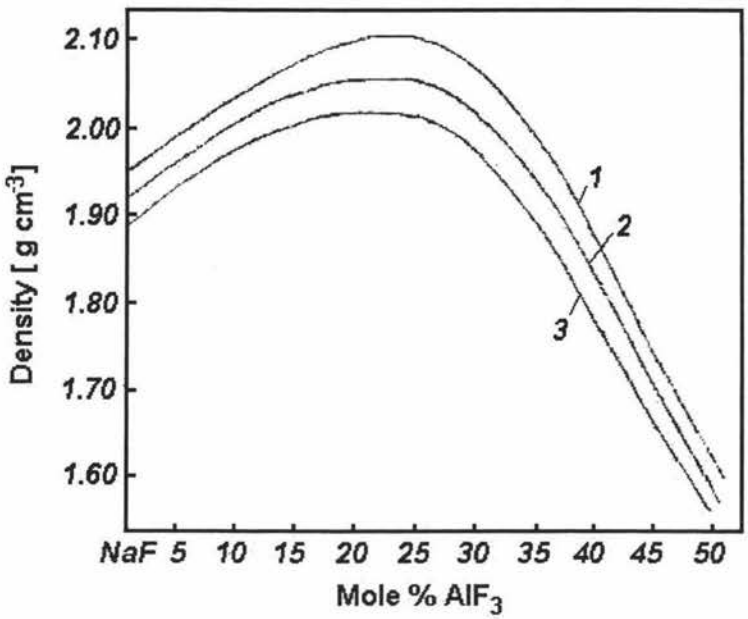

Figure 1.3 Densities of NaF-AlF_3 Mixtures [23],
(1) 1000 °C, (2) 1050 °C, (3) 1100 °C

1.3.7 Current and Energy Efficiency

The previous sections have looked at how the bath composition, in particular the cryolite ratio, can affect many chemical and physical properties of the electrolyte. These properties are important when considering the current and energy efficiency of the process.

The current efficiency is defined as the ratio between the actual metal output (kg/Amp) and the theoretical aluminium output (kg/Amp). According to Faraday's law, the theoretical output of aluminium is calculated at 0.3354 g/Amp. Most industrial cells operate with high current efficiency values of between 85 % and 95% [24].

The energy efficiency is simply defined as the ratio of actual energy input (kWh/kg Al) and the theoretical energy required (kWh/kg Al). Using the thermodynamics for the reduction of alumina to aluminium it is found that the theoretical energy requirements are 5.64 kWh/kg Al for an isothermal process. Currently all industrial smelters operate with energy efficiencies below 50%.

Equation 1.8 gives the overall specific energy consumption.

$$E = \frac{2.980 * V}{x} \qquad (1.8)$$

where: E = Specific energy consumption [kWh/kg Al]
V = Cell voltage
x = Current efficiency

As discussed in section 1.3.3, the current efficiency is primarily affected by the re-oxidation of dissolved aluminium. Bath temperature is considered to be one of the most influential variables that can be used to increase the current efficiency by reducing this re-oxidation rate [25]. Operating at low cryolite ratios, by the addition of AlF_3, is one way of reducing the liquidus temperature of the melt.

The cell voltage, which appears in Equation 1.8, is the result of three different contributions:

- The decomposition voltage which provides the energy for Equation 1.1
- Polarisation voltage at the electrode-electrolyte interfaces
- Voltage drops due to the resistance of cell components (electrodes, electrolyte etc.)

Section 1.3.5 described how the electrical conductivity of the electrolyte and therefore voltage drop, is affected by the bath composition and temperature. Improving the electrical conductivity can reduce the voltage drop and therefore increase the overall energy efficiency.

Bath composition, namely the cryolite ratio, is therefore a vital variable that can be used to maximise the current and energy efficiency of the smelting process.

1.4 Changes in the Cryolite Ratio

As shown in the previous sections the bath composition, especially the cryolite ratio, influences many variables within the Hall-Héroult cell. Therefore it is important to select an electrolyte composition that will optimise the process, to give high aluminium production rates with low operating and capital costs. However this selection of bath composition is not the end of the problem: the bath composition in industrial smelter cells continuously changes with time. Generally there is a net decrease in the AlF_3 concentration (i.e. a net increase in CR) with approximately 20 kg of AlF_3 consumed per tonne of aluminium produced [25]. Reasons for this change are given in the following sections.

1.4.1 Reactions of Electrolyte with Impurities

There are many impurities that enter the cell during the process of producing aluminium. These impurities include various metals oxides and usually enter the cell during the addition of alumina. The following equation shows how these impurities can react with the electrolyte to change the composition of the bath. This leads to a net decrease in the AlF_3 concentration.

$$6NaF.2AlF_3 + 3MO \rightarrow 3MF_2 + Al_2O_3 + 6NaF \qquad (1.9)$$

where: M is a divalent metal such as Ca or Mg

1.4.2 Reaction of Electrolyte with Moisture

Moisture can also enter the cell and react with the electrolyte. Equation 1.10 shows the reaction between cryolite and water, leading to a decrease in the AlF_3 concentration. Hydrogen fluoride is also released adding to the fluoride loss from the cell.

$$6NaF.2AlF_3 + 3H_2O \rightarrow 6HF + Al_2O_3 + 6NaF \qquad (1.10)$$

1.4.3 Side Ledge Changes

As discussed in paragraph 1.3.4, side ledge changes can effect the composition of the electrolyte, as the side ledge is rich cryolite. When this frozen ledge is re-melted or dissolved into the bulk of the electrolyte, it will increase the overall cryolite ratio of the cell. Likewise there will be a decrease in the cryolite ratio during the formation of the side ledge. It has been estimated that a change of ± 20% in the side ledge mass can effect the AlF_3 concentration by ± 2% for a certain cell type [26]. Side ledge changes occur when the heat balance of the cell is disrupted by events such as the anode effect, material addition to the cell, or cell voltage changes.

1.4.4 Evaporation and Dusting of Electrolyte Species

The evaporation of various electrolyte species can also change the composition of the bath. The major vapour species is considered to be $NaAlF_4$ [27], which will cause an increase in the cryolite ratio of industrial electrolytes. Hydrogen fluoride gas is another component found in the exhaust gas. This gas originates from the reaction between the electrolyte and water (Equation 1.10). Entrainment of electrolytic species in the anode gas is the other contributor to fluoride loss in industrial cells [27]. These entrained species may either be in a liquid or solid state.

1.4.5 Time Lag and Overfeeding

It has been reported that there is a time lag between the addition of AlF_3 and the resulting change in the AlF_3 concentration [28]. This time lag can be anywhere between several hours and several days in length [28,29]. Because of this time lag, cell operators can overreact to AlF_3 concentration measurements, resulting in excessive AlF_3 addition and eventually a lower than expected cryolite ratio [28]. This overreaction may also occur when the cryolite ratio gets to low and soda is added to correct the baths composition.

1.5 Electrolyte Composition Measurement

As discussed is section 1.4, the cryolite ratio of industrial electrolytes, continuously changes with time. Currently there is no in situ method for accurately measuring the cryolite ratio. As seen in section 1.3, the cryolite ratio affects many bath variables, so fast and accurate measurement of the cryolite ratio is important in order to control these variables. A brief description of various techniques used for cryolite ratio and bath composition measurements is given below.

1.5.1 Traditional Wet Chemical Analysis

There are many chemical methods that can be used to determine the cryolite ratio of the electrolyte. Typical methods include:

- Pyro-titration [30]
- Titration with $AlCl_3$ [31,32]
- Titration with $Th(NO_3)_4$ [31,32]

Pyro-titration is performed on acidic electrolyte samples (i.e. CR< 3) by first adding a known quantity of NaF to a molten sample. The excess AlF_3 present in the sample reacts with the newly added NaF, forming cryolite. The neutralisation point of the titration can be determined by dripping an indicator such as phenolphthalein or bromothymole blue on to a cooled portion of the sample. Once this neutralisation point is reached, the mass of NaF used in the pyro-titration can be used to calculate the excess AlF_3 percentage or cryolite ratio.

Volumetric titration of the cryolite ratio firstly involves the selective dissolution of NaF and AlF_3 containing compounds in a NaOH solution. A known excess of standardised NaF solution is added and the solution neutralised with HCl, followed by saturation with NaCl. The aluminium present in the solution forms cryolite, and the remaining excess F^- is titrated with an $AlCl_3$ solution while boiling, using eriochrome cyanamide

as the indicator. This method is used for AlF_3 rich samples typically giving the cryolite ratio with an accuracy of ± 0.4 - 0.6 units [32].

The titration of excess F^- using thorium nitrate is another method of determining the cryolite ratio of an electrolyte sample. For samples rich in AlF_3, the sample is first sintered with a measured quantity of NaF at 600-800 °C for at least 20 minutes. During this process the excess AlF_3 is converted to cryolite. Depending on the cryolite ratio, the excess AlF_3 can be in the form of chiolite ($Na_5Al_3F_{14}$) ($1.65 < CR < 3$) or both chiolite and AlF_3 ($CR < 1.65$) [6]. If the electrolyte sample is basic ($CR > 3$) no sintering step is needed.

$$2Na_5Al_3F_{14} + 8NaF \rightarrow 6Na_3AlF_6 \qquad (1.11)$$

$$AlF_3 + 3NaF \rightarrow Na_3AlF_6 \qquad (1.12)$$

The sinter is finely ground and leached with water to dissolve the remaining NaF. The excess of F^- is titrated with $Th(NO_3)_4$, using sodium alizarin sulphonate as the indicator. This method gives highly reproducible results with a typical accuracy of ± 0.1 units [31,32]. The problems with this method arises from the sintering reaction which is required when analysing acidic electrolytes. At the high temperatures used in this sintering step, AlF_3 rich species such as $NaAlF_4$ can be lost as a vapour. This loss results in the measured cryolite ratio being overestimated.

These traditional chemical methods are generally time consuming and labour intensive due to the nature of the reactions involved, and can suffer from lack of reproducibility [32].

1.5.2 Instrumental Analysis

There are several instrumental techniques, which can determine the composition of the electrolyte. These include atomic absorption spectroscopy, x-ray diffraction, and x-ray fluorescence and Fluoride selective electrodes.

Atomic absorption spectroscopy is a very common technique of determining the concentrations of a wide range of elements in a solution, providing a relatively quick analysis of a sample using instruments that are relatively common in most laboratories. The benefit of atomic absorption spectroscopy is that no sintering or melting the sample is required.

Provided that the alumina content of a sample is known, the cryolite ratio could be calculated simply by analysing a solution containing the dissolved electrolyte sample, for both sodium and aluminium. Other compounds including calcium, magnesium and lithium fluoride could also be measured this way.

A method has also been described where by the excess aluminium fluoride is first reacted with potassium chloride in the presence of fluoride ions, as shown by Equation 1.13 [33].

$$AlF_3 + KCL_{excess} + F^- \rightarrow K_3AlF_6 + KCl \qquad (1.13)$$

Once the reaction is complete, the remaining potassium chloride is determined by flame atomic absorption spectroscopy. This method enabled cryolite ratios between 2.4 and 3 to be determined, with a standard deviation of ± 0.9-3.4% [33]. This method may be considered simpler than other atomic absorption techniques as only potassium needs to be analysed and the alumina content does not need to be known.

X-ray diffraction and x-ray fluorescence are considered more useful than the other instrument techniques as the analysis can be performed directly on solidified samples taken from the bath [32]. X-ray diffraction identifies compounds from characteristic diffraction patterns each compound produces. The intensity of the peaks within the diffraction pattern is related to the amount of that particular compound present in the sample. When a sample of electrolyte is taken from the bath, a range of crystalline compounds form upon cooling, as shown below [32].

- Cryolite (Na_3AlF_6)
- Chiolite ($Na_5Al_3F_{14}$)
- Calcium Cryolite ($NaF.CaF_2.AlF_3$)
- Fluorite (CaF_2)
- Sodium Fluoride (NaF)
- Alumina (Al_2O_3)
- Lithium Cryolite (Li_3ALF_6)
- Aluminium Fluoride (AlF_3) at CR < 1.65 [6]

The cryolite ratio can be determined by comparing the intensities of a certain cryolite peak and a peak from chiolite, as the majority of excess AlF_3 crystallises as chiolite [32]. An internal standard method of determining the cryolite ratio by x-ray diffraction has also been discussed and showed good agreement with a titration technique [34]. However when electrolytes with high AlF_3 concentrations (above 24wt%), are solidified, AlF_3 is also crystallised, making this method unsuitable these electrolytes [35].

X-ray fluorescence may be used to determine the concentration of elements within the electrolyte. Like x-ray diffraction the solid sample must be prepared in a consistent way to ensure results are comparable. There are also some inter-elemental effects, which must be considered when analysing the result. X-ray fluorescence has been successful in determining the cryolite ratio, CaF_2, and Al_2O_3 concentration of low temperature electrolytes [35].

Fluoride selective electrodes are another way that the cryolite ratio of an electrolyte sample can be determined [30,36]. Fluoride selective electrodes provide a potential response to the free F^- present in a solution, which is typically logarithmic in respect to concentration.

For acidic (CR<3) samples, the excess AlF_3 is reacted with NaF to produce cryolite before the remaining sodium fluoride is determined using the fluoride selective electrode. This reaction can be performed in aqueous solutions [36] or by sintering the sample with the sodium fluoride at high temperature as shown by equations 1.11 and

1.12 [30]. Sintering at high temperature can result in the volatilisation of AlF_3 rich species, so this needs to be considered. Once the excess AlF_3 has reacted, the potential of the solution is measured using a fluoride selective electrode. The potential is compared to a standard curve to determine the quantity of NaF remaining, allowing the cryolite ratio to be calculated. This method has been found to give results in good correspondence to other methods such as X-ray diffraction [36], pyro-titration and the thorium nitrate titration [30].

1.5.3 Using other Bath Variables

From measurements of bath and liquidus temperature, it is be possible to calculate the cryolite ratio provided the content of alumina and other additives is known. Temperature measurements have been used for calculating the excess AlF_3 concentration in industrial cells [25,37-39]. There are probes available for liquidus temperature [40] and alumina content [41] measurement in industrial cells. This method of cryolite ratio measurements could be developed further although currently liquidus temperature and alumina content measurements are not widely performed in industrial cells. A method utilising differential temperature measurement has also been suggested as a method by which the cryolite ratio or alumina content can be measured [42]. Bath resistance has also been used in a model to control the AlF_3 content of industrial electrolytes [25].

1.5.4 Electrochemical Measurement

Electrochemical measurements of cryolite ratio changes, have been made in cryolite-alumina melts using liquid aluminium and sodium alloy electrodes [3]. The galvanic cell used for measuring the cryolite ratio is shown below.

$$Al / NaF - AlF_3 - Al_2O_{3(sat)} / Pb - Na_{(xNa \approx 0.05)} \qquad (1.14)$$

This corresponds to the following overall cell reaction:

$$3NaF + Al \rightarrow 3Na + AlF_3 \qquad (1.15)$$

with the following Equation describing to potential between the electrodes:

$$E = E^0 - \left(\frac{RT}{nF}\right)\ln\left(\frac{(a_{AlF3})(a_{Na})^3}{(a_{NaF})^3(a_{Al})}\right) \qquad (1.16)$$

where: E = Potential difference between electrodes [V]
E^0= Standard Potential of the cell [V]
R = Gas constant, 8.314 [J/mol.K]
T = Temperature [K]
n = Number of electrodes involved
F = Faraday constant, 96490 [C/mol]
a_x = activity of species x

Assuming the activities of the aluminium and sodium electrodes remain constant this equation simplifies to:

$$E = E_c - \left(\frac{RT}{nF}\right)\ln\left(\frac{(a_{AlF3})}{(a_{NaF})^3}\right) \qquad (1.17)$$

where: E_c is a constant potential term

This shows that a change in the ratio of the AlF_3 and NaF activities (i.e. a change in the cryolite ratio) will correspond to a change in the measured potential between an aluminium and sodium alloy electrode.

The basic equipment set-up used for these electrochemical measurements is shown in Figure 1.4.

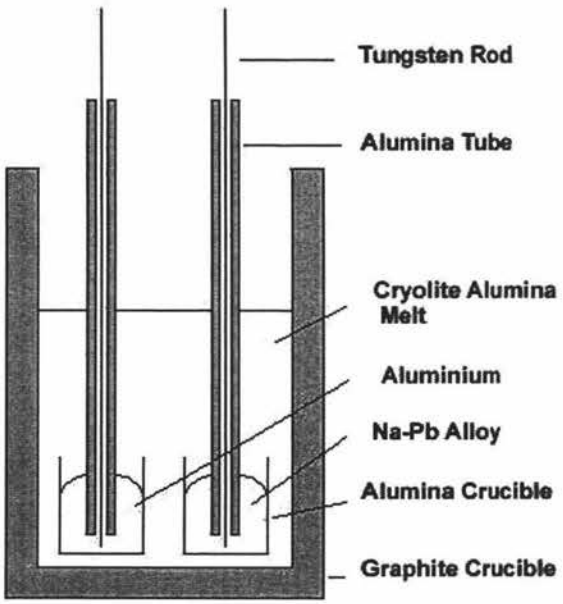

Figure 1.4 EMF cell set-up [3].

The results from this work showed that the potential could indeed be used to measure the cryolite ratio changes, however problems with the stability of the electrodes were found [3]. The activities of the electrodes, in particular the sodium alloy electrode, were found to change with time [3]. This was suggested to be due to the dissolution of sodium into the molten electrolyte [3]. Aluminium was also found within the sodium alloy electrode and is believed to be due to the reaction shown by Equation 1.18 [3].

$$3Na + AlF_3 \rightarrow 3NaF + Al \qquad (1.18)$$

Although the liquid pool electrodes have stability problems in cryolite-based melts, it is believed that electrochemical measurement of the cryolite ratio is possible, provided that stable electrodes can be constructed. The benefit of an electrochemical method to determine the cryolite ratio would be the speed and ease of obtaining the results.

Several other workers [43] have carried out other electrochemical measurements in cryolite-based melts using galvanic cells. One such cell as shown below was used to measure the activity data for the $NaF\text{-}AlF_3\text{-}Al_2O_3$ system [44].

$$Pb\text{-}Na \,/\, Na_3AlF_{6\,(l)}\ \alpha\text{-}Al_2O_{3\,(sat)} \,/\, \alpha\text{–}Al_2O_3 \,/\, NaF_{(l)}\ AlF_{3\,(diss)}\ \alpha\text{-}Al_2O_{3\,(sat)} \,/\, Pb\text{-}Na \qquad (1.19)$$

The cell shown in Equation 1.19 gave quite stable potential measurements for cryolite ratios above 2, and the potential was found to be a linear function of the cryolite ratio [44]. The sodium-lead alloy used was found to be a reliable sodium electrode with the relative change of the measured potential being typically ±0.1 mV/hr [44].

Activity data for AlF_3 and NaF in cryolite based melts have been reported in literature to some degree [44-47]. These activity measurements will enable the theoretical potentials or potential changes to be calculated, for cells similar to those shown by equation 1.14. The activity of NaF and AlF_3 has been calculated as a function of the cryolite ratio (Figure 1.5).

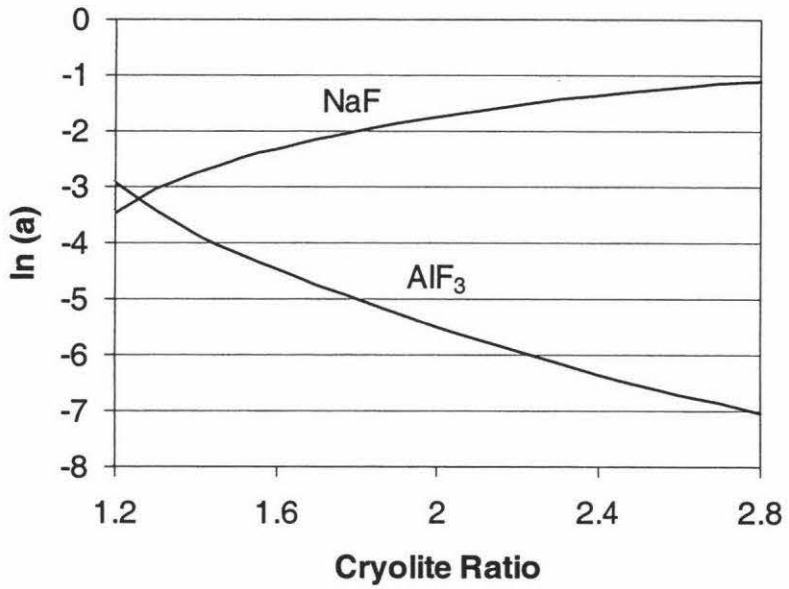

Figure 1.5 Activity of NaF and AlF_3 in the NaF-AlF_3 system, as a function of CR at 1300 K [46]

1.6 Electrodes for Electrochemical Sensors

As discussed above, it is critical that stable electrodes are used when constructing a system to make potentiometric measurements of the cryolite ratio. In order to test electrode stability the potential between the electrode in question, and an electrode that is known to be stable must be measured. Provided that this measured potential is stable over some period the electrode can be considered stable. If a stable test electrode does not exist, the electrode in question should be compared to another identical electrode [48]. Variation from a potential difference of zero indicates a lack of stability.

1.6.1 Liquid Metal Electrodes

As discussed in section 1.5.4, electrodes constructed using static pools of liquid metal have been partly successful for electrochemical measurements in laboratory cells [3]. These can suffer from dissolution and contamination reactions (Equation 1.18), which prevents these electrodes, particularly liquid sodium alloy electrodes, from remaining stable over any extended period in cryolite melts. It has been shown that aluminium electrodes constructed using a wetted molybdenum hook design, have good stability in cryolite melts [48]. Several authors [48,49] have also described liquid aluminium electrodes where the aluminium is allowed to sit above a density-modified bath containing high levels of BaF_2.

1.6.2 Gas Electrodes

Gas electrodes have been successfully used to determine the activity of species within a cryolite melt [43]. These electrodes usually incorporate a platinum wire or carbon rod, over which a gas such as oxygen, carbon monoxide, or carbon dioxide is flushed. It is felt that these electrodes should be avoided due to difficulties when used in industrial cells [3].

1.6.3 Solid Electrodes

There are some solid electrodes that have been used for electrochemical measurements in cryolite based melts [43]. These electrodes can be constructed from various metal oxides and aluminium alloys [43]. These electrodes are reported to suffer from corrosion and stability problems, due to the extreme conditions found in industrial electrolytes.

1.6.4 Dropping Metal Electrodes

Dropping metal electrodes have been used in electrochemical experiments since Kucera first developed them in 1903 [50]. They have traditionally been used for polarography, which was developed by Heyrovsky in 1922 [51]. Polarography is linear sweep voltammetry, carried out at a dropping electrode. This electrode consists of a reservoir and a fine capillary (ID < 1 mm), from which the liquid metal is allowed to drip into the electrolyte (Figure 1.6). The drop of metal provides the electrical contact with the electrolyte.

Polarography allows the changes in current resulting from the electrolysis of a solute, to be followed by a dropping electrode and an increasing applied voltage [52]. As the voltage sweeps, there will be a point at which a metal ion will be reduced. As this occurs the current increases sharply until the diffusion-limited current is reached at which point the current levels off [53]. Small polarographic maxima can also be observed in the polarogram, when the current exceeds the diffusion-limited current for a short period. This is suggested to be due to the streaming or convection of the electrolyte around the growing electrode drop [53]. These polarographic curves have been widely used for quantitative analysis of both inorganic and organic solutes [53] as well as analysis of molten salts [54].

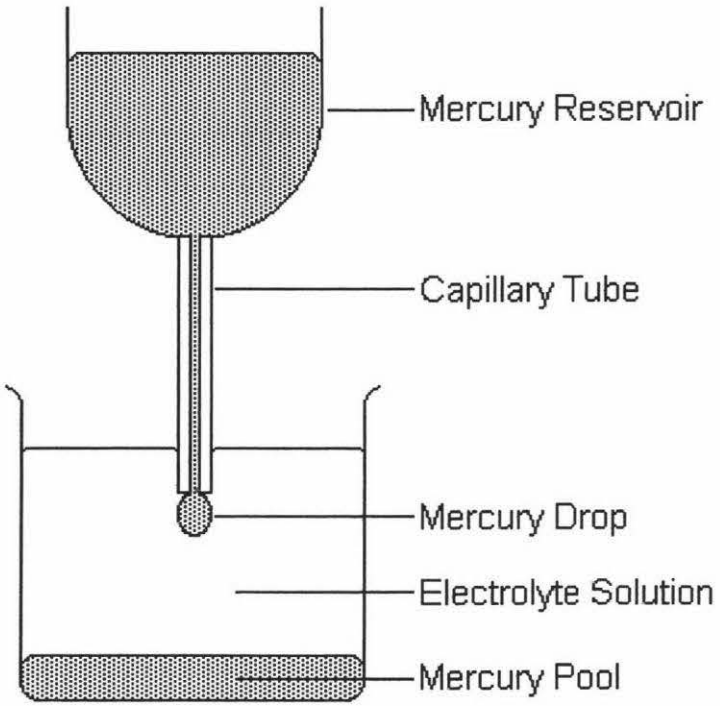

Figure 1.6 Dropping Metal Electrode Schematic

Dropping metal electrodes usually use mercury as the electrode metal, as this is liquid at room temperature, although molten metals such as lead [55,56], bismuth [55,57] silver [57,58] and gold [57] have been used at higher temperatures.

The benefit of using dropping metal electrodes is the continuously renewing electrode surface at the drop-electrolyte interface. This means that reactions between the electrolyte and the electrode metal do not affect the activity of the electrode, as any surface contamination or dissolution is lost when the drop falls away from the capillary.

The Hagen-Poiseuille Equation, as shown below, gives the flow rate of liquid metal from the capillary tube.

$$m = \frac{\pi r^4 \rho P}{8 l \eta} \qquad (1.20)$$

where m = Mass flow rate of liquid metal [kg/s]
r = Internal radius of capillary [m]
ρ = Density of liquid metal [kg/m^3]
P = Pressure of liquid metal head [Pa]
l = Length of capillary [m]
η = Viscosity of liquid metal [Pa.s]

The drop's formation will be restricted due to the surface tension of the electrolyte-metal interface. This is described as the back pressure on the drop, as given by Equation 1.21.

$$P_{back} = \frac{2\gamma}{r} \qquad (1.21)$$

where: P_{back} = Back pressure on drop [Pa]
r = radius of drop at any time [m]
γ = electrode-metal surface tension [N/m]

In most applications of dropping metal electrodes, the electrode is designed to give 10-60 drops/min [53] at an overall flow rate of 1-4 mg/sec [52]. There are some methods that have been used to control the dropping rate or flow rate of metal, by using mechanical drip dislodges [59], and pressure head control [52,56,57]. There are several texts available that fully cover polarography and polarographic techniques [52,59].

Currently it is believed that dropping metal electrodes have only been used in electroanalytical techniques where a signal such as a voltage is actively applied to the cell in order to measure a response. They have not been utilised in a galvanic or passive cell set-up in order to measure the potential between two electrodes such as in potentiometry.

This type of electrode may be useful in a system to make potentiometric measurements of the cryolite ratio. The discussed activity changes of the sodium electrode could be avoided, if a sodium alloy is used as the metal in the dropping electrode.

1.7 Objectives of Work

As shown by section 1.3 the cryolite ratio, can effect many variables with an industrial smelter cell, including the overall efficiency of the aluminium production process. Currently only laboratory based methods such as X-ray diffraction, are used to measure the cryolite ratio. As these methods have a time lag between sampling and measurement, cryolite ratio control based on these methods is difficult. A sensor that can measure the cryolite ratio in situ would greatly improve the ability for cryolite ratio control.

The Objectives of this work are as follows:

- Develop liquid metal electrodes for electrochemical cells
- Investigate cryolite ratio measurement using electrochemical cells
- Develop dropping metal electrodes for cryolite melts
- Investigate dropping metal electrodes in electrochemical cells

2 Cryolite Ratio Measurement

There are many different methods for determining the cryolite ratio of aluminium smelter electrolytes. In this chapter, some of these methods will be discussed and examined in respect to their performance and application to industrial smelters. The major consideration for cryolite ratio measurement in an industrial setting is the speed and reliability of the method. Although some techniques may provide highly accurate results, this accuracy must be weighed against the time needed to perform such analysis. However, slow techniques that provide accurate results are still valuable as reliable calibration and checking methods.

2.1 Electrolyte Samples

All electrolyte samples used in this work were prepared by accurately weighing together pure cryolite, technical grade AlF_3 (6.5 wt% Al_2O_3), and pure Al_2O_3. It was felt necessary to ensure that electrolyte samples contained Al_2O_3, as all industrial electrolytes would have some Al_2O_3 present. As the AlF_3 used contained some Al_2O_3 this was taken into consideration when making up the various electrolyte samples. In some cases pure AlF_3 was used to determine the effect of Al_2O_3 on the experimental results. The compositions chosen for analysis were typically of cryolite ratios 1.2, 1.6, 2.0, 2.4, and 2.8, with 3 wt % Al_2O_3. This wide range was chosen to reflect the traditional composition of industrial electrolytes as well as including the low ratio electrolytes that are increasing in interest [35]. Electrolyte samples were sintered together at just below their liquidus point for 1 hour, in a platinum crucible.

2.2 Fluoride Selective Electrode

The measurement of the cryolite ratio by the fluoride selective electrode method is based on the response of the electrode to solutions of NaF. The method is best suited to basic electrolytes (those which contain excess NaF i.e. CR >3) but can be modified for

acidic electrolytes (those which contain excess AlF_3, i.e. CR < 3). The potential of a solution made from an electrolyte sample is measured using a fluoride selective electrode. This potential is compared against a standard curve made form NaF standard solutions to determine the excess NaF (or CR) in the electrolyte sample. For acidic electrolytes the excess AlF_3, is first reacted with an known quantity of NaF. The remaining NaF in solution is determined from the measured potential, allowing the amount of NaF reacted and therefore the excess AlF_3 of the electrolyte sample to be calculated.

The reaction between the excess AlF_3 and the added NaF forms cryolite as shown by equations 2.1 and 2.2. Depending on the cryolite ratio, the excess AlF_3 can be in the form of chiolite ($Na_5Al_3F_{14}$) (1.65 < CR < 3) or both chiolite and AlF_3 (CR < 1.65) [6].

$$2Na_5Al_3F_{14} + 8NaF \rightarrow 6Na_3AlF_6 \qquad (2.1)$$

$$AlF_3 + 3NaF \rightarrow Na_3AlF_6 \qquad (2.2)$$

These reactions have been performed by sintering the sample with NaF [30,31] or boiling a sample in a NaF solution [36].

2.2.1 Experimental Method

A set of NaF standard solutions with concentrations ranging from 200 to 2000 mg/L was made up into 100 ml volumetric flasks. 5 ml aliquots of these solutions were diluted with 45 ml of a 58.5 g/L NaCl solution in 125 ml conical flasks. These were allowed to equilibrate to 30°C in a water bath. The potential of each solution was read using an Orion combination fluoride selective electrode (model 96-09-00) connected to an Orion Research Ion-analyser (model 701A) to obtain a standard curve.

Electrolyte samples were finely ground with a mortar and pestle to less than 100 μm. Approximately 0.8 g of accurately weighed electrolyte sample, was then sintered in a small silica crucible with an accurately weighed amount of NaF. Sintering temperature was 800 °C with a sintering time of 30 minutes. Once the sample had been sintered with the NaF, the sinter was finely ground to less than 100 μm, then placed in a 200 ml volumetric flask and made up to the mark with distilled water. A 5 ml aliquot was taken and diluted with 45 ml of a 58.5 g/L NaCl solution in a 125 ml conical flask. The solution was allowed to equilibrate to 30°C in a water bath before the potential was read using the fluoride selective electrode. Equations 2.3 to 2.5 show how the cryolite ratio can be calculated from the concentration measurement.

$$NaF_{remaining} = \frac{CV_2V_1}{5} \qquad (2.3)$$

$$AlF_{3reacted} = \frac{(NaF_{Added} - NaF_{remaining})}{1.5} \qquad (2.4)$$

$$CR = \frac{1.2(M - M_{Add} - AlF_{3reacted})}{0.4(M - M_{Add}) + 0.6AlF_{3reacted}} \qquad (2.5)$$

where: C = measured NaF concentration [mg/l]

V_2 = volume of measured solution [l]

V_1 = volume of sinter solution [l]

$NaF_{remaining}$ =Mass of NaF remaining [g]

NaF_{added} = Mass of NaF added to sample [g]

$AlF_{3reacted}$ = Mass of AlF_3 reacted [g]

M = Electrolyte sample mass [g]

M_{Add} = Mass of electrolyte additives i.e. Al_2O_3 [g]

CR= Cryolite ratio

2.2.2 Results and Discussion

The measured potential of the standard NaF solutions was plotted against the logarithm of the NaF concentration (Figure 2.1). It should be noted that the fluoride selective electrode used in this work showed a drift of approximately 2 mV per day at constant NaF concentrations. This must be accounted for by repeating the calibration curve before each set of measurements.

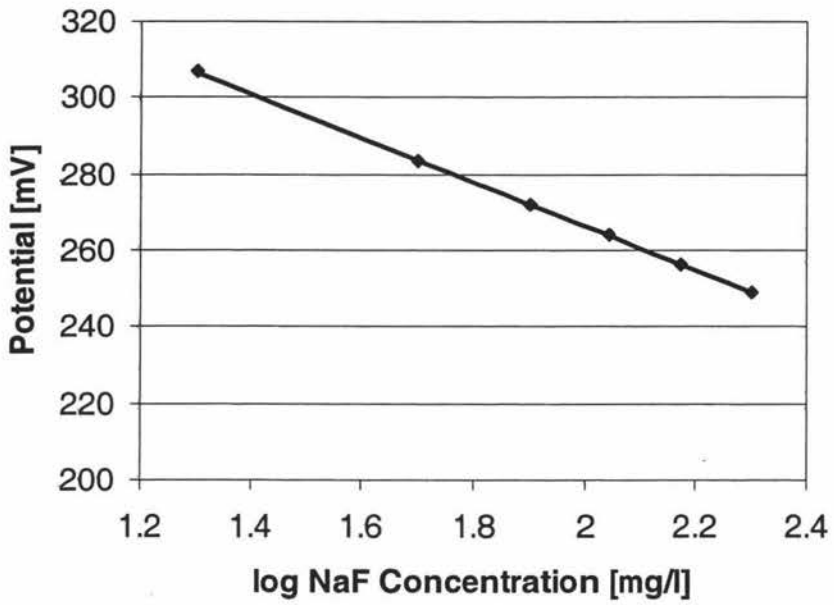

Figure 2.1 Standard Potential - Log NaF concentration curve at 30 °C

The electrolyte samples used in this experimental work were analysed as described above (Table 2.1). It is assumed that the added NaF only reacts with the chiolite and AlF_3 in the samples to form cryolite.

The results show that the concentrations measured by the Fluoride selective electrode are all slightly higher than expected, leading to the cryolite ratio of electrolyte samples being over estimated. This result could occur due to several reasons.

- Sintering Reactions not complete
- Electrode response to species other than NaF
- Error in potential readings
- Loss of AlF_3 rich species during experimental procedure

The cause of these errors were further investigated as described in the following.

It has been widely documented that the reactions that occur during the sintering process (shown by Equations 2.1 and 2.2) completely convert the chiolite or AlF_3 to cryolite within 30 minutes at the temperatures used in this work [30-32]. To confirm this, X-ray diffraction was carried out on the sintered samples, to check for traces of chiolite or AlF_3, which would show whether the sintering reactions were complete. The X-ray diffraction technique is described in section 2.4. The diffraction patterns obtained for the sinters, showed peaks for both cryolite and NaF, but did not show the characteristic peaks for either chiolite or AlF_3. The x-ray diffraction patterns for two sinters (original CR=1.6 and 2.4) are shown in the Appendix. This shows that all of the available chiolite and AlF_3 were converted during the sintering process. This analysis does not explain why the measured NaF concentrations were consistently higher than expected. Another possible explanation may be that impurities within the samples can react with the chiolite or AlF_3 thus reducing the mass of NaF reacted. One such impurity is CaF_2, which would form calcium cryolite upon reaction with chiolite or AlF_3.

In an attempt to improve the reaction completion, the sample and NaF was pressed into a tablet to increase the contact between the sample and NaF particles. This procedure increased the bulk density of the sinter from approximately 1.6 g/cm^3 to 2.25 g/cm^3. This method however showed a decrease in the percentage of reacted AlF_3, leading to an increase in the calculated cryolite ratio. This may be due to selective particle settling during the tabulating process, resulting in an uneven distribution of the NaF and electrolyte, lowering the observed percentage of AlF_3 reacted.

Table 2.1 Fluoride Selective Electrode Results

Cryolite Ratio	Mass Sample [g]	Mass AlF_3 in sample [g]	Mass NaF added [g]	Potential [mV]	Concentration [mg/l]	Remaining NaF [g]	Reacted AlF_3 [g]	% Reacted AlF_3	Calculated CR
1.2	0.7435	0.2705	0.4892	285.5	46.51	0.0930	0.2641	97.6	1.23
1.6	0.8638	0.2172	0.5045	266.8	98.01	0.1960	0.2057	94.7	1.65
2.0	0.6987	0.1130	0.4119	260.3	127.00	0.2540	0.1053	93.2	2.06
2.4	0.7240	0.0638	0.4055	255.2	155.60	0.3112	0.0629	98.4	2.41
2.8	0.7827	0.0211	0.4327	248.3	203.30	0.4066	0.0174	82.6	2.83

Table 2.2 Effect of Sintering Conditions

Sintering Conditions	Cryolite Ratio	% AlF_3 Reacted	Calculated CR
Standard	2.0	93.2	2.06
Tabulated	2.0	80.4	2.16
Sinter Time 1 hr	2.0	82.7	2.14
Low Sample:NaF Ratio	2.0	88.7	2.09

Another attempt was made to improve the completion of the reactions, by increasing the sintering time to 1 hour. This resulted in a decrease in the apparent percentage of reacted AlF_3, which indicates a loss of an AlF_3 rich species from the sinter during the procedure (Table 2.2). This could be by evaporation of $NaAlF_4$, which is the principal volatile species found in cryolite systems [27]. In order to minimise this possible loss, the sintering reaction should be carried out either at a lower temperature or with a reduced sintering time. These however can effect the overall reaction rate and completion, resulting in the cryolite ratio being over estimated.

The ratio of electrolyte sample to added NaF was also examined. Reducing the sample to NaF ratio from 1:0.6 to 1:0.3 has little effect on the reacted AlF_3 percentage and calculated cryolite ratio (Table 2.2).

As the sintering reaction was carried out in silica crucibles, there may be some reactions between the silica crucible and the excess AlF_3. Results obtained using a platinum crucible gave similar results to those in which silica crucibles were used, indicating that any reactions which may occur, have little effect on the final result.

Repeated analysis indicated that the precision in the readings were ± 0.01 cryolite ratio units for CR < 2, and ± 0.05 cryolite ratio units for CR > 2. This difference in precision is most likely a result of changes in the measured concentrations error due to the logarithmic nature of the standard curve. At the low concentration end of the standard curve, ± 0.5 mV results in a precision of around ± 0.4 mg/l in the measured concentration. Comparing this with a precision of approximately ± 4 mg/l at the high concentration end, it can be reasoned that there is more error associated with potential measurements at higher NaF concentrations. This indicates that it is necessary to have similar final NaF concentrations prior to using the fluoride selective electrode to avoid this variance in the precision of the measured concentration. Such a technique has been used [30] with the initial addition of NaF being proportional to the excess AlF_3 to ensure that the final NaF concentrations are similar. Although this technique has its advantages it should be noted that possible errors could arise resulting from the differing degrees of homogeneity during the mixing of the electrolyte sample and the added NaF prior to sintering. It is thought that keeping the ratio of electrolyte to added NaF the same, such mixing issues should be minimised.

The presence of additives in the electrolyte samples will add to the error in the accuracy of the results obtained by this method. As the excess AlF_3 is measured (or excess NaF in basic electrolytes), the content of other compounds such as Al_2O_3 and CaF_2 must be known in order to calculate the cryolite ratio (see Equation 5.5). These additives can lead to overestimating the cryolite ratio if they are not accounted for (Table 2.3).

Table 2.3 Effect of Additives on CR measurement

Measured CR	Actual Cryolite Ratio		
	1 wt %	2 wt %	5 wt %
1.2	1.188	1.177	1.140
1.6	1.590	1.576	1.548
2.0	1.992	1.984	1.958
2.4	2.395	2.389	2.372
2.8	2.798	2.796	2.790

Although the experimental results indicate that the method may tend to overestimate the cryolite ratio this could be reduced by generating the standard curve from electrolyte samples with known cryolite ratios. This would reduce the error resulting from incomplete reactions or AlF_3 loss. The repeated analysis indicates that the fluoride selective electrode method of measuring the cryolite ratio can give highly reproducible results with high precision. In respect to this method's suitability to industrial control or monitoring, it is thought that the sintering step is too time and labour intensive. Typically the analysis time was approximately 45 minutes per sample, although more than one sample can be prepared simultaneously reducing the overall time required. This method should be considered as a valuable calibration technique for methods that are less labour and time intensive.

2.3 Cryolite Ratio Measurement by NaF Conductivity

This method is based on the electrical conduction of NaF solutions. It is possible to determine the cryolite ratio of a basic electrolyte (i.e. CR > 3) by simply dissolving the excess NaF present in the sample and measuring the electrical conductivity of the aqueous solution using a conductometer. As in the fluoride selective electrode method,

this method can be modified to suit acidic electrolytes (i.e. CR < 3) by first reacting the excess AlF_3, with a known amount of NaF. The remaining NaF is determined by the electrical conductance allowing the excess AlF_3 present in the original sample to be calculated.

2.3.1 Experimental Method

A set of standard NaF solutions of the range 500-7000 mg/L were made by taking aliquots of a 20 g/L NaF solution and diluting them with distilled water in 100 ml volumetric flasks. The standard solutions were placed in 150 ml beakers and allowed to equilibrate to 22°C in a water bath. The electrical conduction of the solution was measured using a digital YSI (30/10FT) conductometer.

Electrolyte samples were finely ground with a mortar and pestle to less than 100 μm. Approximately 1 g of accurately weighed electrolyte sample, was then sintered in a small porcelain crucible with an accurately weighed amount of NaF. The temperature was held at 800 °C and the sintering time kept to 30 minutes. Once the sample had been sintered with the NaF, the sinter was finely ground to less than 100 μm, then placed in a 100 ml volumetric flask and made up to the mark with distilled water. The electrical conductance of the resulting solution was measured using the same method as the standards.

2.3.2 Results and Discussion

An electrical conductivity standard curve was obtained for the NaF standard solutions (Figure 2.2).

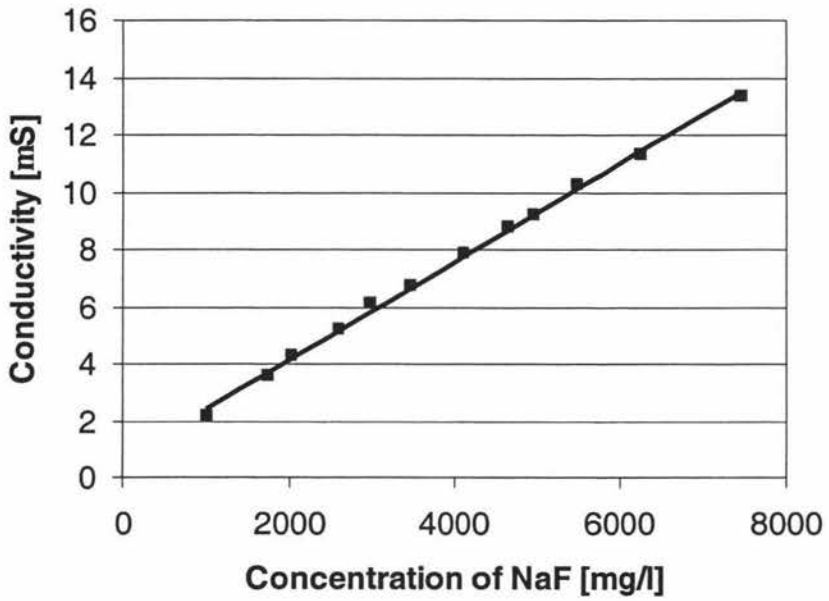

Figure 2.2 Electrical Conductivity Standard Curve of NaF solutions

The conductance of a NaF solution is seen to be linear over the concentration of 500 – 7000 mg/l. This enables a wide range of cryolite ratio samples to be examined using this one standard curve.

The results obtained from the analysis of a range of cryolite ratios are shown in Table 2.4. These results indicate that this method gives a good estimate of the cryolite ratio of a wide range of electrolyte compositions. Repeated experiments gave errors of approximately ± 0.02 cryolite ratio units. Over the range examined, like the fluoride selective electrode method, the cryolite ratio is normally over estimated by the analysis. This is most likely due to either incomplete sintering reactions or loss of AlF_3 during the process as described in the fluoride selective electrode method. It should be noted that if the conductivity standard curve were generated from cryolite ratio standards there would be greater accuracy, as the errors caused by the incomplete sintering reactions and AlF_3 loss will be accounted for. Typically the procedure could be performed in 40 minutes.

Like the fluoride selective electrode method, this method is suggested as a calibration tool only, due to the time required for the procedure.

Table 2.4 NaF Conductivity Results

Cryolite Ratio	Mass Sample [g]	Mass AlF_3 in sample [g]	Mass NaF added [g]	Conductivity [μS]	Remaining NaF [g]	% Reacted AlF_3	Calculated CR
1.2	1.0255	0.385	0.7557	4140	0.5591	96.92	1.20
1.6	1.0080	0.260	0.5599	4190	0.3609	92.07	1.65
2.0	1.0251	0.171	0.3898	3535	0.2230	87.02	2.08
2.4	0.9934	0.0901	0.2969	3830	0.1156	85.34	2.46
2.8	0.9970	0.028	0.2076	4000	0.0312	75.11	2.84

2.4 X-Ray Diffraction

X-ray diffraction of cryolite based electrolytes is a very common technique used in industrial smelters for cryolite ratio measurement. This technique allows the identification of compounds within a solid sample from the characteristic diffraction pattern each compound produces. The intensity of the diffraction pattern is proportional to the amount of the compound within the sample, which enables x-ray diffraction to be used for quantitative as well as qualitative analysis. The expected d-spacings of the main peaks for the important compounds within an electrolyte sample are summarised below (Table 2.5)

Table 2.5 XRD Peak Locations

Compound	Important Peak d-spacings
Cryolite	4.55
Chiolite	5.82
AlF_3	3.54
Al_2O_3	2.09

This technique allows the cryolite ratio to be calculated from the ratio of selected cryolite and chiolite peak intensities. Firstly, cryolite ratio standards are analysed and a polynomial expression is derived, relating the intensity ratio to the cryolite ratio of the standard. From this polynomial expression, the cryolite ratio of bath samples can be calculated from their intensity ratios. Normally this method gives results, which are both accurate and relatively quick, and therefore is the method of choice for many industrial smelters. The main problem arises when the cryolite ratio of the sample drops below approximately 1.65. In these AlF_3 rich electrolytes, as well as chiolite, AlF_3 is also crystallised during solidification [35], preventing the normal quantitative measurement technique from being used.

2.4.1 Experimental Method

The samples were finely ground in a mortar and pestle to less than 150 μm. The samples were then loaded into back pack powder holders before being loaded into the x-ray diffraction sample rack. Most x-ray diffraction equipment allows multiple samples to be analysed reducing the labour aspect of the analysis. In this work a Phillips PW 1710 Automatic Powder X-Ray Diffractometer with a cobalt tube (wavelength 1.79026 nm) was used to analyse the samples. The intensities for the d-spacings between 10 and 1.64 Å were measured for each sample and the pattern plotted on a chart recorder.

2.4.2 Results and Discussions

The diffraction patterns were recorded for electrolyte samples of cryolite ratios 1.2, 1.6, 2.0, 2.4, and 2.8, all with 3 wt% alumina (Appendix). The important peaks [32] for cryolite and chiolite were located and their intensities measured (Table 2.6). For the cryolite ratio standards of 1.2 and 1.6, the AlF_3 peaks were also assigned. For the intensity ratio analysis, it was decided to use the peaks located at 4.55 Å and 5.82 Å for cryolite and chiolite respectively. The intensity ratio was then plotted against the cryolite ratio and a polynomial expression fitted (Figure 2.3).

Table 2.6 XRD Peak Intensities

Cryolite Ratio	Peak Intensities		Intensity Ratio (Chiolite / Cryolite)
	Cryolite (4.55 Å)	Chiolite (5.82 Å)	
2.0	558	568	1.018
2.4	1117	310	0.278
2.8	1335	58	0.0434

The results show that intensity ratio correlates well to the cryolite ratio and can be used with confidence to calculate the cryolite ratio. Unlike the other two methods tested in this work, this method relies on comparing samples to a standard curve generated from standards of known cryolite ratio.

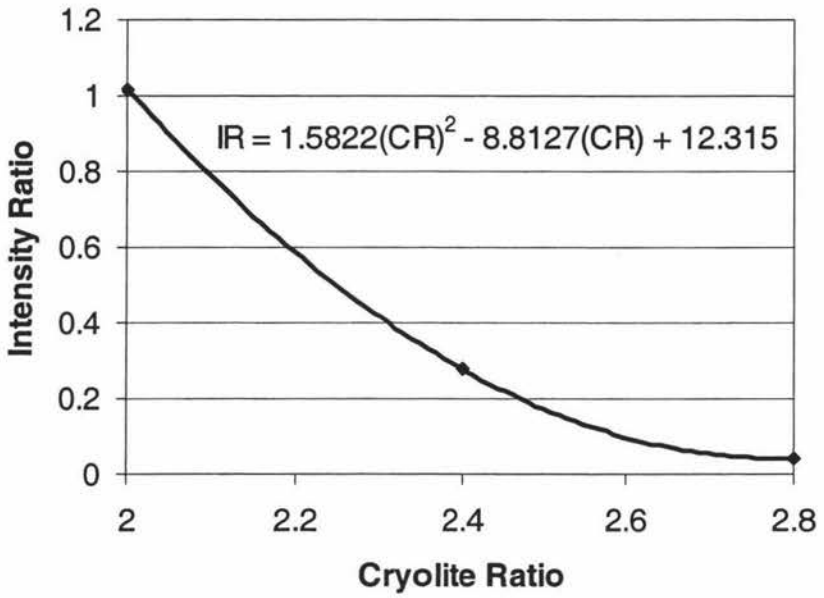

Figure 2.3 Intensity Ratio vs. Cryolite Ratio

As expected the intensity ratio for the cryolite ratios of 1.2 and 1.6, did not fit within the polynomial expression due to the presence of AlF_3 as well as chiolite in the solidified sample. This is clearly evident in the diffraction patterns obtained for samples of cryolite ratio 1.2 and 1.6.

As this method is widely used in many industrial smelters for cryolite ratio control, there is considerable literature concerning its reproducibility and accuracy [31,32,34]. Due to the high cost of this analysis, it was felt unnecessary to further examine cryolite ratio measurement via this method. However as mentioned x-ray diffraction was also used to analysis intermediates in the fluoride selective electrode method (2.2.2) and evaporated electrolyte (5.2.1).

Even with this short investigation of cryolite ratio measurement by x-ray diffraction, it is clear that this method provides much faster results with far less labour contributions, than the other two methods investigated. The high cost of this analysis prevented it from being used as the cryolite ratio measurement technique for the remaining portion of this work.

2.5 Overall Conclusions

The results indicate that all three methods are suitable for cryolite ratio measurements of typical industrial electrolytes. The first two methods are also suitable for measurements of electrolytes rich in AlF_3 (e.g. CR=1.2 and 1.6), whereas x-ray diffraction is only suitable for electrolytes where chiolite contains the majority of AlF_3 (CR>1.65). Provided that careful experimental procedures are followed, the fluoride selective electrode gives a very high degree of reproducibility with an error of ± 0.05 cryolite ratio units. Although the error associated with the X-ray diffraction method was not investigated, from the work of others [31,32,34] it is thought that this analysis is the most suitable for typical industrial electrolytes. Analysis time is considerably less for the x-ray diffraction method, than for the fluoride selective electrode and NaF conductivity methods, which require sintering reactions and solutions to be made up. X-ray diffraction was too expensive to be used for further bath analysis, so the fluoride selective method will be used throughout the remaining work.

3 Development of Electrodes

As discussed in chapter 1, the cryolite ratio may be measured using two electrodes (sodium and aluminium) to set-up a simple electrochemical cell. The potential measured between these two electrodes is related to cryolite ratio of the molten electrolyte. The electrodes must first be developed and tested, to ensure stable measurements can be made.

3.1 Definition of Electrode Types

Two basic types of electrodes are used throughout this work. The first type is a simple a liquid metal pool in contact with the electrolyte and held within an inert container. This will be referred to as a static electrode. The second is based on a dropping metal electrode, similar to those used in polarography, and will be called the dropping metal electrode.

3.2 Materials of Construction

3.2.1 Environment Considerations

Cryolite based melts are highly corrosive towards most commonly used materials such as metals and glass. The high operating temperatures (960-1000 °C) needed when using cryolite based electrolytes, further rule out materials with low working temperatures. The materials should also be relatively robust to withstand typical industrial operating standards.

3.2.2 Electrode Body Materials

Commonly, graphite is used as the main material in which cryolite based electrolytes are contained. Graphite however is an electrical conductor, which cannot be used to

hold the electrode metal if it is also in contact with the electrolyte as it will set up a short-circuited galvanic cell [43]. Boron nitride is a electrically insulating ceramic commonly used in laboratory based Hall-Héroult experiments. This ceramic is easily machined and resists cryolite based melts and high temperature very well. Quartz has also been used in several experiments [60] although this will dissolve into the cryolite melt to some degree [61].

3.2.3 Electrode Metals

The electrode metals used in this work are standard analytical grade sodium and aluminium. Analytical grade tin and lead are also used to alloy with the sodium metal. Bismuth alloys were ruled out as bismuth expands upon freezing, which would cause damage to the electrode body. In later designs the aluminium was also alloyed with tin. Molybdenum wire (99.95 % purity) was used as the contact wire in all electrode designs.

3.2.4 Preparation of Electrode Alloys

The alloying metal was heated in a small porcelain crucible by a muffle furnace. The furnace was filled with oxygen free nitrogen gas to reduce any oxidation reactions. The temperature of the molten metal (either Pb or Sn) was maintained at 350-400 °C before the addition of the sodium metal. The sodium was accurately weighed into liquid paraffin oil to ensure no unnecessary contact between moisture in the air and the highly reactive sodium took place. Before adding the sodium to the alloying metal, the excess paraffin oil was removed from the metal using dry blotting paper. The alloy was stirred using a dry molybdenum wire loop, before small rods of the alloy were cast into a stainless steel mould. The sodium content of the alloys ranged between 2 and 10 mole percent.

The aluminium-tin alloy was prepared in similar conditions, however the furnace temperature was maintained at 800 °C. The aluminium alloy contained 25 wt% aluminium.

3.3 Development of Static Electrodes

The static electrodes used in this work can be described as simple liquid metal pool electrodes and are similar to many electrodes used in molten salt and other high temperature environments. These electrodes are constructed around a small pool of molten electrode metal (Figure 3.1). This electrode pool is held within an electrically insulating material, and is in contact with the electrolyte bath via an opening in the insulating material. A connecting molybdenum wire is in contact with the electrode pool, but is not in contact with the electrolyte bath

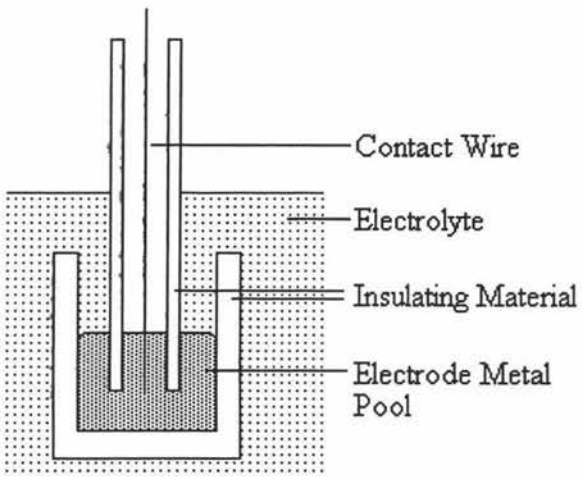

Figure 3.1 Typical Static Electrode Schematic

This chapter will examine the development of two similar liquid metal electrodes, the aluminium electrode and the sodium alloy electrode. The use of these electrodes in cryolite based melts has been discussed in literature, with some construction details mentioned [48,49].

Although Figure 3.1 shows the typical arrangement of the static electrodes used in this work, two variations were developed to try and achieve a design suitable for industrial use and provide a lifetime suitable for its application. Early electrodes were easily damaged by the extreme conditions, with the electrodes lifetime only being several minutes.

Due to the activity changes in the sodium electrode as discussed in literature [3], it was decided that the sodium alloy should be easily removed and replaced after each experiment. As the sodium electrode is based on alloys with low melting points, such as Pb-Na and Sn-Na, the electrode metal could be heated and poured from the electrode body after each experiment.

Two designs of this static type electrode were examined (Figure 3.2). The difference in designs is that closed tube design has no opening through the boron nitride to the cryolite melt. Provided that the boron nitride is porous and the electrolyte can wet the boron nitride, the electrolyte will contact the molten electrode pool setting up the desired electrochemical cell.

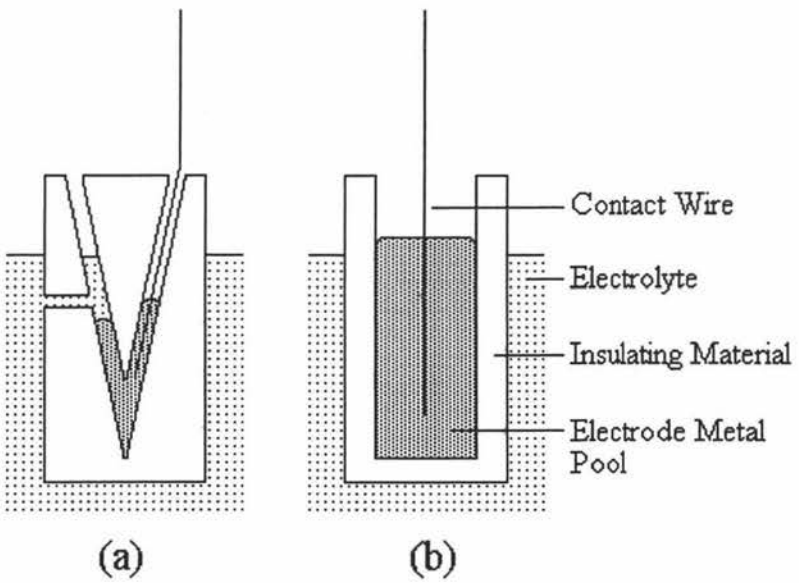

Figure 3.2 Different Static Electrode designs, (a) Open V Design, (b) Closed Tube Design

3.3.1 Construction Details for Static Electrode Deisgns

Both of these two electrode designs were constructed from hot pressed boron nitride rod of diameter 9.5 mm, with an overall length of 60 mm.

The V shaped reservoir in the Open V design, was constructed by machining two holes of 3 mm diameter into the boron nitride rod at such an angle so that the holes met approximately 5mm from the base of the rod. A side hole of diameter 1mm was also machined into the boron nitride rod 20 mm from the base, to enable the electrolyte to contact the electrode metal.

The Closed Tube design was simply constructed by machining a 7 mm hole down the length of the boron nitride rod to a depth of 55 mm. This resulted in a wall thickness of 1.25 mm.

Each electrode body was slowly heated to 600 °C to ensure any moisture within the boron nitride was driven off before the electrode metal was added to the electrode. The electrode metal was placed within the electrode body in the form of small rods 2 mm in diameter and 20mm in length. The molybdenum wire was carefully cleaned and inserted into the boron nitride body. Contact between the electrode metal and the molybdenum wire was established once the electrode metal melted after the electrode was placed into the hot furnace.

3.4 Development of the Dropping Electrode

As previously mentioned, it is believed that dropping metal electrodes are currently used solely in polarography. Typically mercury is used as the electrode metal, however there has been work carried out using various molten metals at higher temperatures [55-58]. The main benefit of the dropping electrode is the continuously renewing electrode surface that minimises the activity changes due to reactions with the electrolyte and dissolution of the electrode species. This electrode may solve the problems of sodium activity changes, which has been discussed in relation to static electrodes previously used cryolite melts [3]. As the sodium electrode is considered to be most prone to activity changes, this work will look at the use of sodium alloys in a dropping metal electrode assembly.

Due to the nature of the cryolite-based electrolyte found in aluminium smelter cells, the construction and materials used for a dropping metal electrode in this environment must be carefully selected. Likewise the control of dropping rate and drop time will be equally complicated by the extreme conditions of an industrial smelter cell.

3.4.1 Hagen – Poiseuille Equation

The mass flow rate of dropping electrodes is described by the Hagen - Poiseuille equation (Equation 3.1). This relationship describes the mass flow of the dropping metal in terms of the capillary dimensions and electrode metal properties.

$$m = \frac{\pi r^4 \rho P}{8 l \eta} \qquad (3.1)$$

where m = Mass flow rate of liquid metal [g/s]
r = Internal radius of capillary [m]
ρ = Density of liquid metal [kg/m^3]
P = Pressure of liquid metal head [Pa]
l = Length of capillary [m]
η = Viscosity of liquid metal [Pa.s]

This equation has been successfully applied to both low temperature mercury systems [59] and high temperature molten salt-molten metal systems [58]. As discussed previously, typical dropping electrodes have mass flow rates of around 1-20 mg/sec. As seen in equation 2.1, the radius of the capillary effects the flow rate considerably due to the fourth power relationship. Because of this, it is important to select a capillary internal radius that will allow for a suitable flow rate. Typically dropping mercury capillaries have internal radii of 0.05-0.1 mm [59].

3.4.2 Capillary Construction

The primary design feature of a dropping electrode is the capillary. In order to design the capillary dimensions a design mass flow rate must be specified. For this work the

actual mass flow rate is not too critical, as diffusion and convection at the electrode surface is less important than in traditional polarography. However, the mass flow rate must provide a suitable experimental period (i.e. period in which electrode can be used without refilling with sodium alloy) so that the stability of the dropping electrode can be examined. This time will be dependent on the ratio of mass flow rate to reservoir capacity.

As industrial sensors should be relatively small, the maximum reservoir capacity will be set at approximately 20 cm^3. Considering this, and a minimum experimental period of 1 hour, the design volumetric flow rate should be approximately 5.5 mm^3/sec. As the sodium alloy will be made up of primarily lead or tin, the alloy density range will be approximately 7.0 - 10.7 g/cm^3. This corresponds to a design mass flow of between 40-65 mg/sec.

The mass flow rate of molten lead (T=1000 °C) is shown as a function of the internal capillary radius and length, using the Hagen- Poiseuille equation (Figure 3.3).

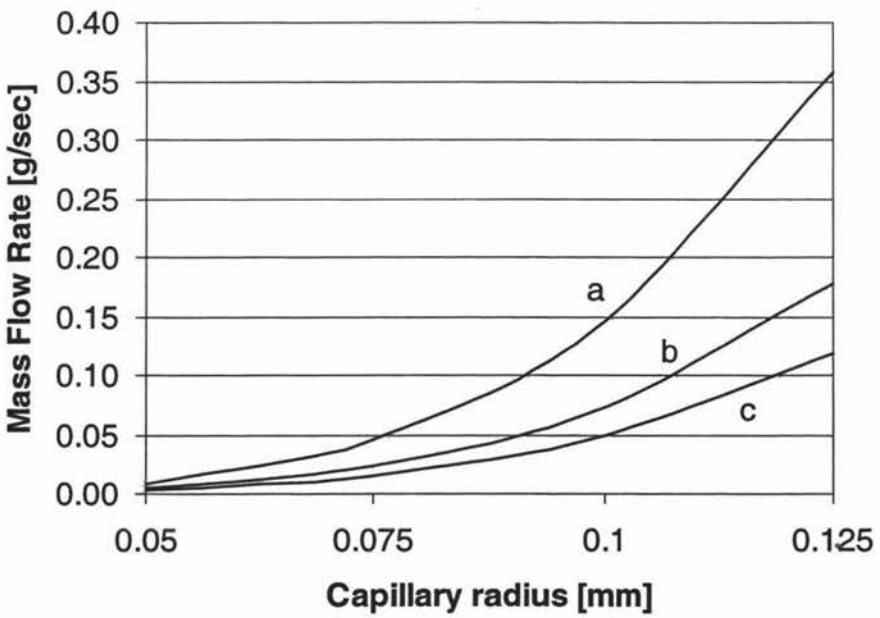

Figure 3.3 Mass Flow rate as a function of capillary radius and length. Pressure head set at 20 cm, (a) l = 50mm, (b) l = 100mm, (c) l = 150mm

It is thought that the capillary radius should be between around 0.07- 0.1 mm, to minimise capillary length, while still maintaining a sufficient radius to avoid blocking and construction difficulties.

The capillary could be purchased from a supplier as in quartz capillaries, or it could be construction from stock material such as hot pressed boron nitride rod. To construct such a capillary, some method of drilling would need to be employed. Standard drilling with a fine drill and laser drilling has been investigated. Using commercially available drill bits, diameters of 0.1-0.2 mm are possible but only at length of between 1-3 mm. Laser drilling of diameters down to 1 μm can be performed quickly and accurately using specialised laser drilling equipment, with a length of up to 30 mm [62]. This laser drilling however is very expensive and was ruled out for this study. Quartz capillary is widely available in a range of both internal and external diameters. Where possible thick walled capillaries should be selected to maximise mechanical strength of the device.

Two dropping metal electrode designs, which could be used in molten cryolite baths, were developed (Figure 3.4). These two designs differ in the construction of the capillary through which the electrode metal flows. The boron nitride tip design utilises conventionally machined hot pressed boron nitride where as the quartz capillary design, simply uses capillaries that can be purchased from glass specialists.

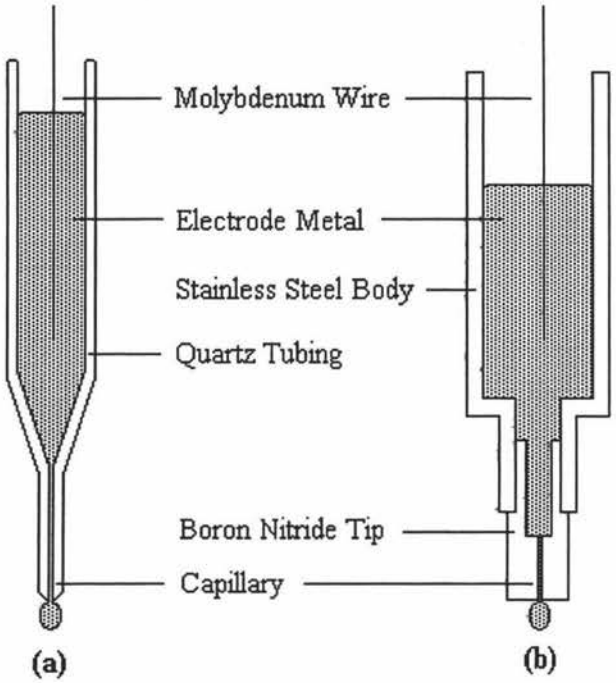

Figure 3.4 Two basic Dropping Metal Electrode Designs, (a) Quartz Capillary Design, (b) Boron Nitride Tip Design

The final designs of these electrodes had internal capillary diameters of 0.2 mm and 0.14 mm for the boron nitride tip design and the quartz capillary design respectively. The capillary length was 3 mm for the boron nitride tip design and 80 mm for the quartz capillary design. The length of the boron nitride tip capillary was restricted by the machining limits using such fine drill bits.

Each design has a reservoir in which the bulk of the liquid electrode metal is stored. The reservoir is connected to the boron nitride tip by screwing the tip into the 253 MA (High Temperature) stainless steel body. A fine thread is used in order to minimise the leakage of liquid metal between the body and tip. The quartz capillary was "welded" to a larger quartz tube, which acted as the reservoir, thus avoiding any possible leakage.

To improve the corrosion resistance of the quartz capillary electrode design, a boron nitride protector was constructed to inhibit the attack of the capillary by the molten electrolyte. The whole assembly was then fitted within a 253 MA stainless steel tube handle.

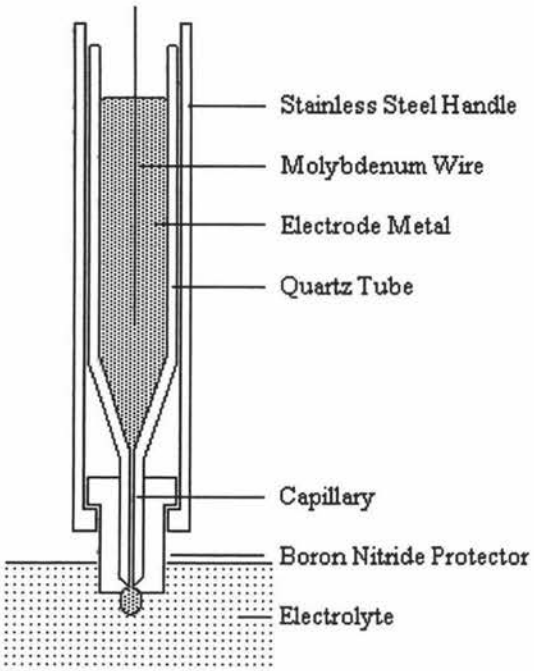

Figure 3.5 Quartz Capillary Electrode Assembly

The molybdenum contact wire was immersed into the electrode metal within the reservoir section of each electrode design. The wire was insulated using alumina tubing, except for the portion immersed into the molten metal. Each electrode was held by a long stainless steel handle, which allowed the electrode to be lowered into the molten cryolite bath.

3.4.3 Dropping Rate Control

The majority of the dropping metal electrodes used are based on the use of mercury as the dropping metal. As this system is used at room temperatures, dropping rate control is achieved by adjusting the pressure head by raising or lowering the reservoir, which is connected to the capillary via rubber tubing. Due to the high temperatures used for cryolite based electrolytes, dropping rate control is considered too complicated for this work and it is suggested that carefully selecting of the capillary dimensions will give satisfactory results.

3.5 Summary of Electrode Development

Throughout the development of these electrodes, both the industrial operation and economic aspects of a possible commercial sensor was considered. The two static electrode designs are based on typical electrodes for potential measurements in molten salts. The dropping metal electrode, using a molten sodium alloy, is thought to be the first use of this kind of electrode in direct potentiometric analysis. Both styles of electrode have been designed in order to be re-usable, by replacing the electrode metal within the electrodes. Chapter 5 will discuss the results from the use of these electrodes in cryolite based electrolytes for the measurement of cryolite ratio.

4 Experimental Methods

4.1 Furnace Arrangement

A schematic of the furnace used throughout this work is shown in Figure 4.1. The main inconel housing is 160 mm in diameter and 440 mm in height and holds the graphite crucible used to contain the electrolyte melt. The furnace is electrically heated by 8 silicon carbide hot rods, spaced evenly around the inconel housing. Two K type thermocouples are used for temperature measurement, with the side thermocouple measurement used to control the heating process. Typically the furnace was heated at a rate of 300 °C per hour until the desired operating temperature was reached. In order to reduce the oxidation of the graphite crucible, a nitrogen atmosphere was maintained within the furnace by passing oxygen free nitrogen gas into the furnace at a flow rate of 0.5 l/min. The electrolyte was continuously mixed throughout most experiments by using a graphite stirrer rotating at 200 – 800 rpm.

4.2 Electrolyte

The cryolite ratio of the electrolyte ranged between 1.2 and 2.8. As alumina was present in the AlF_3 at a concentration of 6.5 wt%, extra alumina was added to the electrolyte to achieve a final alumina concentration in the electrolyte of 3 wt%. Typically around 400 g of electrolyte was used, corresponding to an electrolyte depth of approximately 2-3 cm.

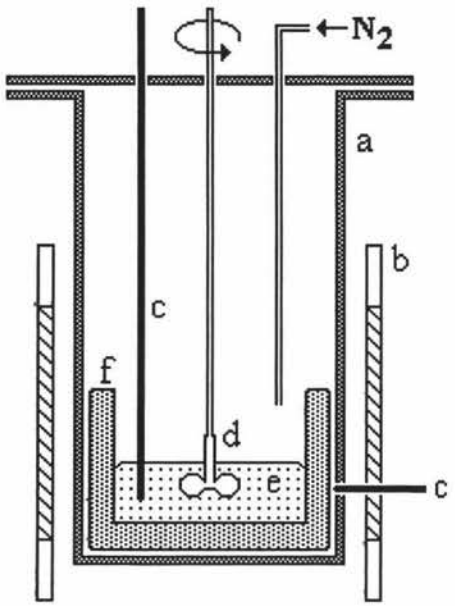

Figure 4.1 Furnace Arrangement. (a) Inconel Housing, (b) Hot Rods, (c) Thermocouples, (d) Graphite Stirrer, (e) Electrolyte, (f) Graphite Crucible

4.3 Electrode Placement

The electrodes were placed in the molten cryolite bath once the operating temperature had been reached. The electrodes were held in place with 253 MA (High Temperature) stainless steel tubes, which were electrically insulated from the electrodes using either boron nitride or alumina separators. These stainless steel tubes protruded through the furnace lid, and were held in place using retort stands and clamps. The molybdenum contact wire was connected to the potential measurement equipment via shielded cabling. The static electrode designs were allowed to touch the base of the crucible containing the molten electrolyte, whereas the dropping metal electrodes were held with the tips approximately 1 cm from the base. Once the experiments were complete the electrodes were removed from the bath before the electrolyte was allowed to cool.

4.4 Potential Measurements

The potential between any two electrodes was measured using a National Instruments LabPC+ data card, installed in a standard desktop computer. The card provided 4 12-bit differential inputs with a voltage range of +5 to -5V. A simple computer program was written to log the measured potentials. 1000 measurements were made, and averaged for every data point recorded, in order to improve the accuracy of the measurements and reduce the effect of any electrical noise. Typically the potential between the electrodes was measured every 20 seconds.

4.5 Cryolite Ratio Measurement

As this work is aimed at developing a sensor to measure the cryolite ratio of a molten electrolyte, a traditional cryolite ratio measurement technique must be used to compare any results obtained and verify an electrolyte composition. In chapter 2 several laboratory techniques were investigated and discussed, and it was decided that the fluoride selective electrode method would be used due to its simplicity and relatively high reproducibility.

4.5.1 Electrolyte Sampling

The electrolyte samples were taken from the experimental cell using two techniques. The first used a small inconel cup attached to a long stainless steel tube. The cup was immersed into the melt and allowed to reach the baths temperature. By constructing the cup with a low thermal mass compared to the electrolyte bath, minimal bath freezing occurred. The small cup was then raised from the bath, and the molten electrolyte sample contained within it was allowed to cool before being removed and finely ground. The second method simply used a solid inconel rod that was dipped into the melt then quickly removed with a layer of frozen electrolyte attached. Provided that rapid cooling occurs, the frozen out sample should reflect that of the bulk electrolyte.

Samples taken using both of these methods were compared using the fluoride selective electrode method. The results indicated that the cryolite ratio of the samples were identical within the error associated with the measurement method. The inconel rod sampling method was normally used to take bath samples, as this had less effect on the overall bath temperature.

4.6 Dropping Rate Measurement

The two dropping metal electrode designs were constructed and tested in respect to the dropping and mass flow rate of the liquid metal. Mercury was used at room temperature to simulate the dropping rate of molten metals such as lead, as this enabled quick results to be obtained while visually observing the electrode. The flow rate of the dropping mercury was measured by hanging the dropping metal electrode from a Mettler digital balance (PB 1501). The mercury was allowed to drop from the electrode and the mass change recorded via an RS-232 serial interface with a desktop computer. This method was also used at high temperature, with the electrode within the furnace and balance situated above the furnace.

4.7 Atomic Absorption of Electrode Metals

The sodium alloys were analysed for concentration changes of sodium by atomic absorption spectroscopy. Approximately 0.05 g of the sodium alloy was dissolved in 15 ml of 1.5 M HNO_3. This solution was then diluted to 500 ml using distilled water, with the final concentration of sodium between approximately 0.5 and 1.0 ppm. Caesium chloride was added to the solution as an ionisation suppressant with a final concentration of 1000 ppm Cs^+. Standards were made up from analytical NaCl and distilled water, with sodium concentrations of 0, 0.25, 0.5, 1, and 1.5 ppm. These standard solutions also contained 1000 ppm Cs^+. The solutions were then analysed by flame absorption spectroscopy using a standard technique, with a lean air-acetylene flame, a slit width of 0.5 nm, lamp current of 5mA, and wavelength of 589.6 nm.

5 Results and Discussion

5.1 Potential Measurements using Static Electrodes

5.1.1 Initial Results – Open V Design

The first static electrodes tested were the open V design (see section 3.3), using Pb-Na (X_{Na} = 5 mol %) and pure aluminium as the electrode metals. When placed in the electrolyte (CR=2.0), a potential between these two electrodes could be measured immediately. A typical potential-time plot for this electrode design is shown (Figure 5.1).

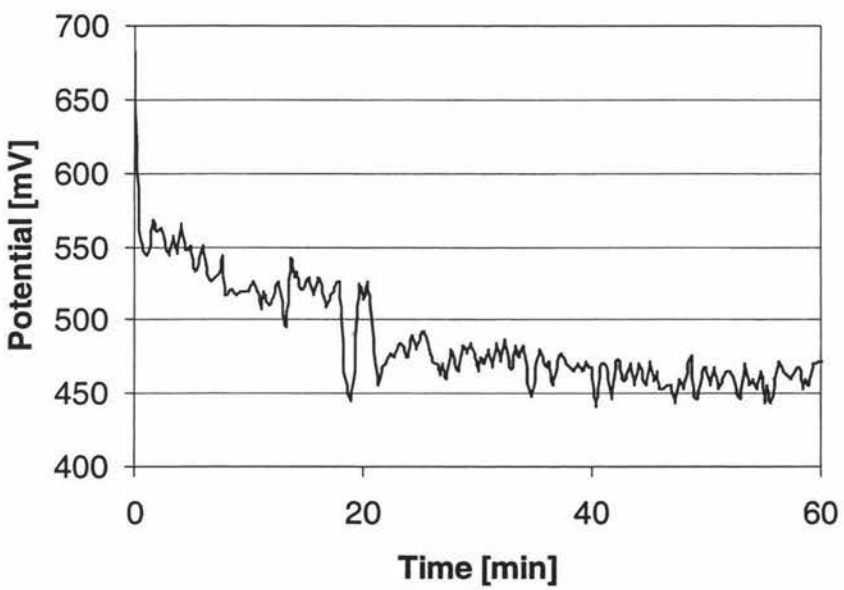

Figure 5.1 Potential vs. Time – Open V design, CR=2, T=1000 °C

The observed potential quickly drops within the first minute, followed by a slow decrease, and then a steady period. Although the measured potential is only stable to within ± 15 mV during the steady period, it shows that the potential measured between these electrode reaches a stable level after 40 minutes. When the electrode is first placed into the molten electrolyte, the bath temperature drops and some electrolyte will most

likely freeze. From the phase diagram (see Figure 1.2), it is seen that cryolite will preferentially freeze if the bath temperature drops just below the liquidus temperature. The potential decrease during this stabilising period is consistent with a decrease in the cryolite ratio, which would occur as a cryolite rich region around the electrodes is mixed back into the bulk of the bath.

5.1.2 Initial Results – Closed Tube Design

The closed tube electrode design (see section 3.3) differs from the open V design, as there is no opening in the boron nitride body through to the cryolite melt. The contact between the electrolyte and electrode is achieved through the wetting of the porous boron nitride by the electrolyte. The potential between a Pb-Na (X_{Na} = 5 mol %) and a pure aluminium electrode was measured over time (Figure 5.2).

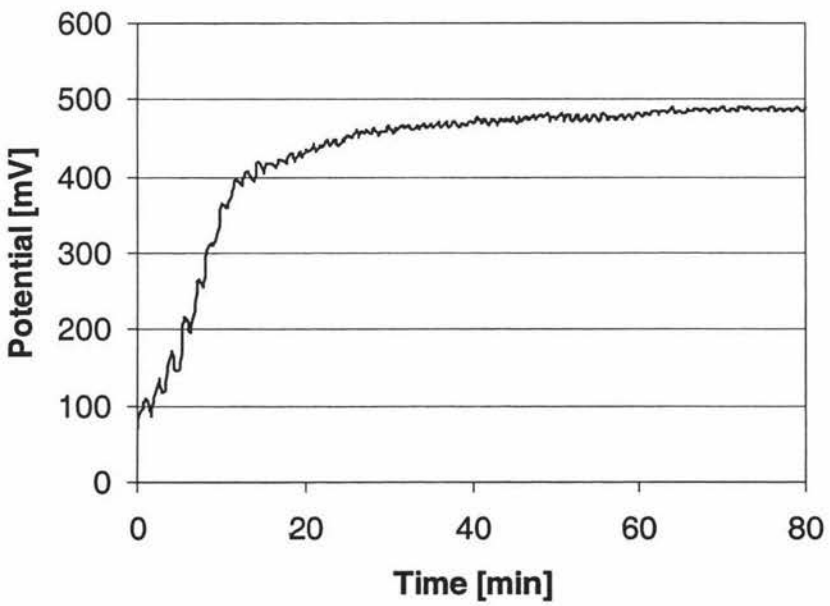

Figure 5.2 Potential vs. Time – Closed Tube design, CR = 2, T = 1000 °C

The time to reach an approximately stable potential is around 40-60 minutes like the result obtained for the open V design. It should be noted that the steady potentials seen in Figure 5.1 and Figure 5.2 both are similar in magnitude which is expected as they were measured in identical electrolytes. However Figure 5.2 shows that the measured

potential started near zero and rose up to the stable potential value. It is thought that this is due to the slow wetting of the boron nitride by the cryolite melt. Due to its manufacturing technique, hot pressed boron nitride contains significant pore volume, which must be first filled by the electrolyte before a potential is measured. This accounts for the initial low potential, as the electrolyte would initially not be in contact with the electrode metal. To examine the pore size distribution, mercury porosimetry was carried out on a fresh piece of boron nitride and a piece of boron nitride which had been immersed in molten electrolyte (CR = 2, Temp = 1000 °C) for two hours. The porosity of the boron nitride is shown as a function of pore diameter (Figure 5.3).

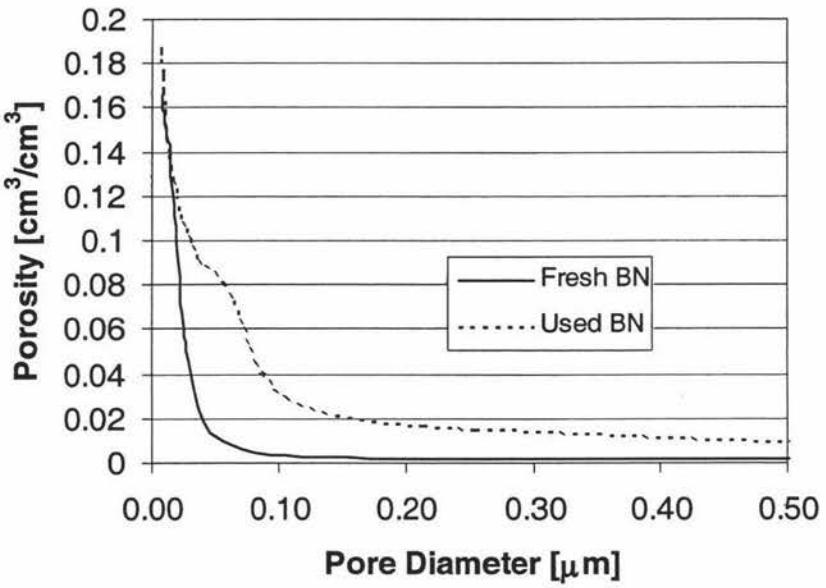

Figure 5.3 Porosity of Hot Pressed Boron Nitride (a) Fresh BN (b) Used BN

The porosity of the fresh boron nitride and the used boron nitride was measured to be 16.5 and 18.7 % respectively. The increase in porosity seen at pore diameters above 0.2 μm in the used boron nitride sample, is probably a result of the molten electrolyte changing the pore structure as it wets the boron nitride. A small amount of inorganic binders are added to boron nitride during its manufacturing process, which may dissolve into the cryolite melt, thus changing the pore structure. Formation of aluminium nitride has also been discussed as a possible cause of boron nitride corrosion [63], and may

cause an increase the porosity of the boron nitride. The surface tension of cryolite melts, which will effect the intrusion of the melt into the pores of the boron nitride, is seen to decrease with increasing AlF_3 concentration [4]. This means that electrolytes with high AlF_3 concentrations will most likely wet the boron nitride quickly providing the necessary contact between the bath and the electrode metal. Scanning electron microscope (SEM) photographs were also taken of both fresh boron nitride and boron nitride which had been immersed in molten electrolyte (CR = 2, Temp = 1000 °C) for two hours (Figure 5.4).

From these photographs it appears that little change occurs in the structure of boron nitride particles after it has been immersed in the molten electrolyte. The photographs do however clearly shows the porous nature of hot pressed boron nitride. This attribute has been utilised in the closed tube electrode design, but may cause problems in the other designs if electrolyte intrusion causes damage to the electrodes.

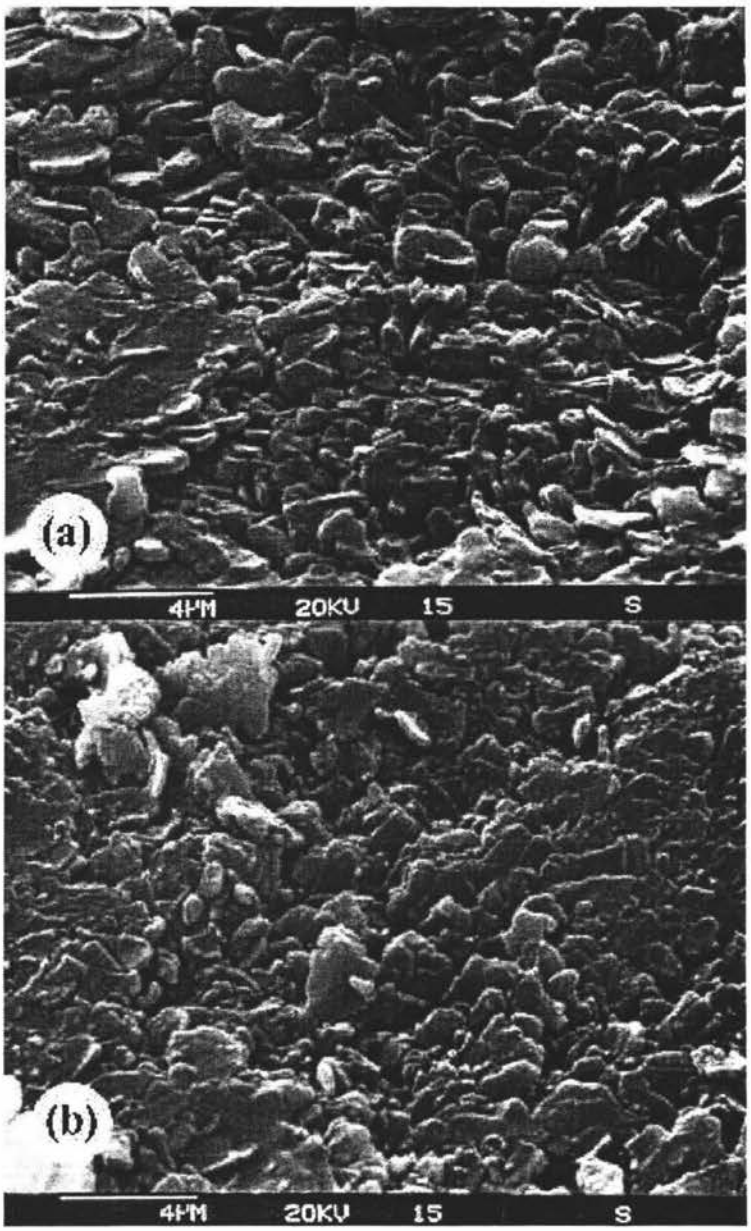

Figure 5.4 SEM Photographs of Hot Pressed Boron Nitride (a) Fresh BN (b) Used BN

5.1.3 Theoretical Potential Changes due to Cryolite Ratio Variance

The potential measured between sodium and aluminium electrodes spontaneously changes with changes in the cryolite ratio (Equation 1.17). The activities of NaF and AlF_3 in cryolite based systems has been discussed in literature to some degree [44-47]. In this work the equations and thermodynamic data provided by Solheim and Sterten [47], were used to calculate the activity of NaF and AlF_3 at various cryolite ratios with an alumina concentration of 3 wt % and temperature of 1000 °C (Figure 5.5).

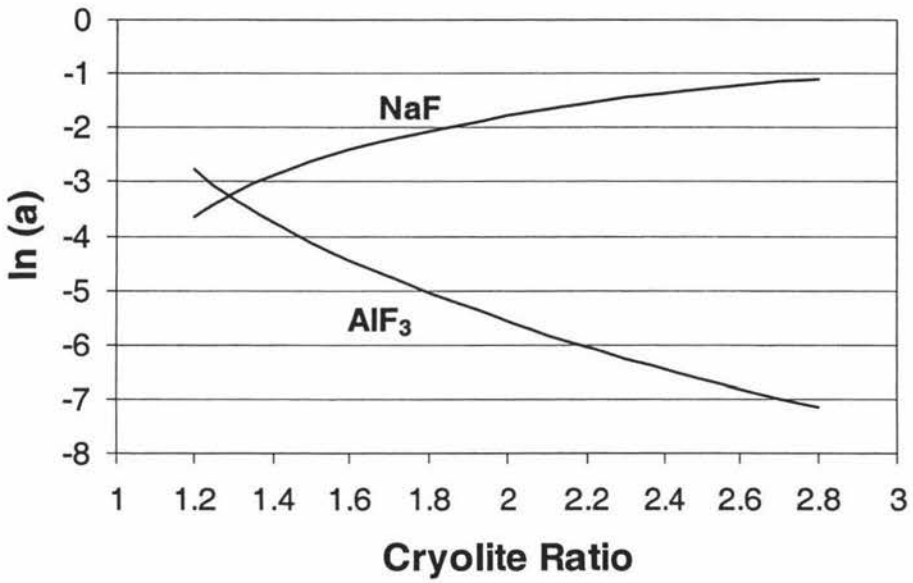

Figure 5.5 Activity data for the NaF-AlF_3-Al_2O_3 system [47]

Using this activity data the change in potential due to cryolite ratio changes at 1000 °C were calculated, using equation 5.1 (Table 5.1).

$$\Delta E = \left(\frac{RT}{nF}\right)\left[\ln\left(\frac{a_{AlF3}^{*}}{a_{NaF}^{3*}}\right) - \ln\left(\frac{a_{AlF3}}{a_{NaF}^{3}}\right)\right] \qquad (5.1)$$

where : ΔE = Potential Change (V)

a^* = activity of species before cryolite ratio change

a = activity of species after cryolite ratio change

R = Gas constant (8.314 J/mol.K)

n = number of electrons in reaction

F = Faradays constant (96500 C/mol)

T = Temperature (K)

Table 5.1 Calculated Potential Changes

Cryolite Ratio Change	Potential Change [mV]
1.2-1.3	68.8
1.6-1.7	31.2
2.0-2.1	21.2
2.4-2.5	15.2
2.8-2.9	11.6

The potential change resulting from a cryolite ratio change of 0.1 units is significantly larger at lower cryolite ratios (Table 5.1). This indicates that the sensor will be more sensitive to cryolite ratio changes in electrolytes with higher AlF_3 concentrations, assuming that the noise or error in the measurements remains constant over the range of electrolyte compositions. In order to measure cryolite ratio changes of 0.1 units over the entire cryolite ratio range used in this work, the sensor and accompanying measurement equipment, must be able to detect potential changes of at least 11.6 mV. To accomplish this, the noise or error in the potential measurements must kept to a minimum.

5.1.4 Experimental Potential Changes due to Cryolite Ratio Change

The effect of an AlF_3 addition to a cryolite melt, on the potential measured between a Pb-Na (X_{Na} = 5 mol %) electrode and an aluminium electrode was examined (Figure 5.6). The addition of AlF_3 corresponded to a cryolite ratio change from 1.9 to 1.6.

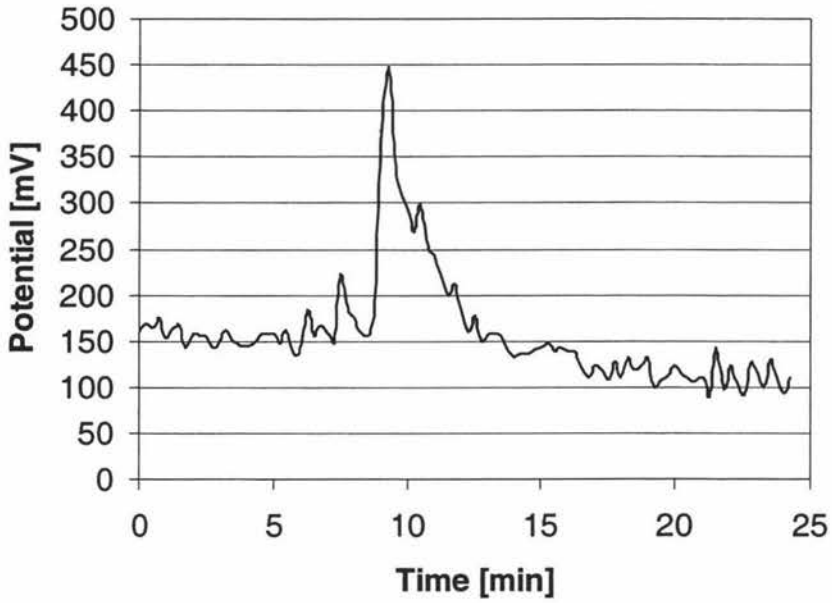

Figure 5.6 Potential vs. Time - Open V design, T=1000 °C, Addition of AlF_3 at 8.5 minutes

It is seen that the potential changes immediately after the addition of AlF_3, and after the initial spike, a lower potential is reached in accordance with the changes in the NaF and AlF_3 activities.

Initially the spike in the measured potential was thought to be a result of bath cooling. To investigate this, the temperature dependence of the activity data and resulting potential was calculated using data from Solheim and Sterten [47] (Figure 5.7). Although a potential spike is consistent with the temperature dependence of the potential in terms of direction, the magnitude of the observed potential spike is some 40 times larger than suggested by the thermodynamic data. The bath temperature during the AlF_3 addition was observed to decrease to around 950 °C, which corresponds to a

theoretical potential increase of approximately 4.5 mV whereas the experimental data shows a spike of around 200 mV. Clearly the temperature alone does not explain this spike in potential, and from this analysis it is seen that bath temperature will have little direct effect on the measured potential. Decreases in the bath temperature however, may result in electrolyte freezing which in turn could alter the composition of the bath temporarily, and even create regions of electrolyte which are heterogeneous in composition. These changes to the bath will affect the potential measured between the electrodes.

The step in potential is seen to be approximately -50 mV, which although is in the correct direction, is significantly lower than the –84.7 mV calculated from the activity data. The difference between these potentials is believed to be a result of unexpected changes in the baths composition during the AlF_3 addition.

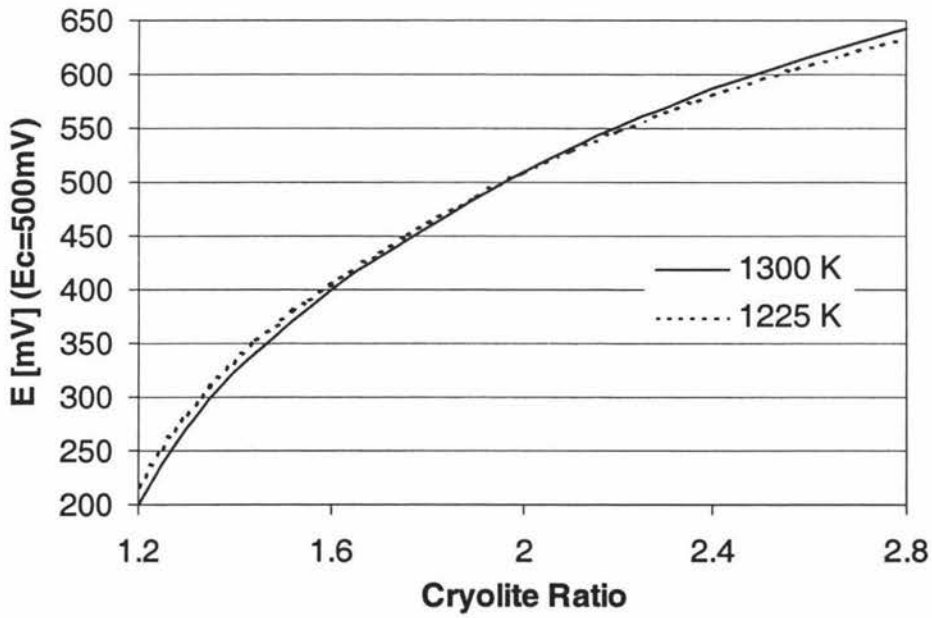

Figure 5.7 Temperature Dependence of the Measured Potential

Further experiments were carried out, and showed that the measured potential changes were typically lower than the changes calculated from the activity data. The potential change, resulting from an AlF_3 addition lowering the cryolite ratio from 1.6 to 1.36 was examined (Figure 5.8).

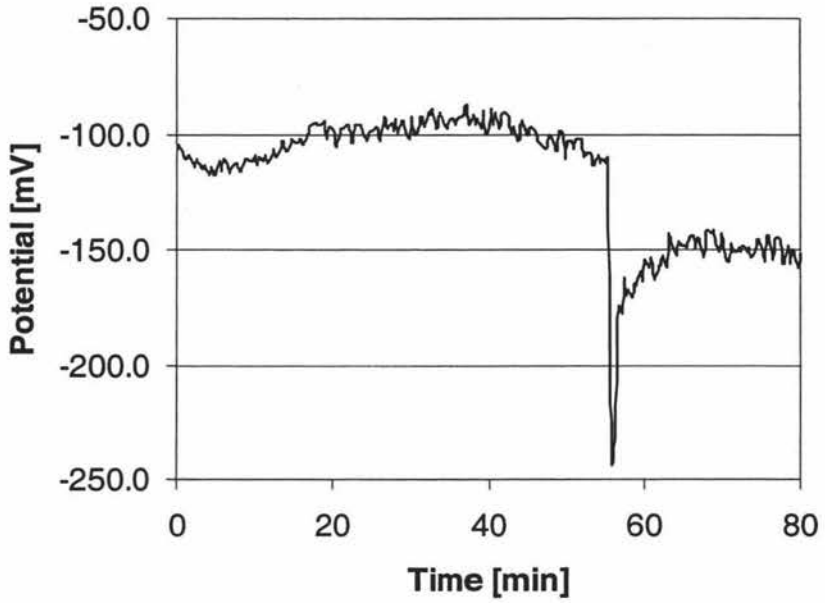

Figure 5.8 Potential vs. Time - Open V design, T=985 °C, Addition of AlF_3 at 55 minutes

The calculated potential change for this AlF_3 addition is –95 mV with the experimental result showing a step of –50 mV. Again it is thought that this significant difference may be explained by unexpected changes in the bath composition.

The immediate effect on the measured potential during the electrolyte addition is different from that observed in Figure 5.6, with a spontaneous decrease occurring immediately after the AlF_3 addition. This difference may arise from localised changes in the cryolite ratio during the AlF_3 addition. The observed decrease in the potential followed by a gradual increase, is consistent with the occurrence of an AlF_3 rich region followed by the mixing of the AlF_3 rich electrolyte into the bulk of the bath. Preferential freezing of cryolite from the bath during AlF_3 additions will add to the formation of an AlF_3 rich region. The dissolution of this frozen cryolite would also result in a gradual increase in the observed potential.

The overall differences in the theoretical and experimental potential changes may also be explained by partial bath freezing. The bath temperature during the AlF_3 addition,

dropped to approximately 960 °C, which is still well above the liquidus temperature for melts of this composition. This bath temperature measurement was made at the thermocouple immersed into the molten bath, and may not necessary reflect the temperature of the entire bath. Further localised cooling therefore may still have occurred around the newly added AlF_3, resulting in partial freezing of the electrolyte. If this frozen of electrolyte fails to dissolve completely, the cryolite ratio after the addition of AlF_3 will in fact be different than that estimated and may take some time to reach the desired level. Changes in the cryolite ratio after a bath addition has been discussed in respect to industrial smelter cells with the observed slow change in the cryolite ratio causing problems in the control of the bath composition [28]. To prevent this the addition of AlF_3 should be carried out in such a way in order to minimise bath freezing. This could be accomplished by making several smaller additions of AlF_3 instead of one addition or preheating of the AlF_3 to reduce the thermal load on the bath. Inadequate mixing could also result in the bath composition being heterogeneous, which would further effect the measured potential. Mixing will also affect the dissolution rate of the added AlF_3 and any frozen electrolyte formed during AlF_3 additions. Mixing effects are discussed in more detail in section 5.2.3.

Bath samples were taken during several experiments before and after bath additions, in an attempt to identify whether cryolite ratio changes were indeed occurring to the magnitude predicted from the bath addition. This could not be performed simultaneously with potential measurements as the potential was disturbed during sample taking. This is most likely due to changes in the thermal balance of the cell as the sample is removed. The samples were analysed using the fluoride selective electrode method, and then plotted to show how the cryolite ratio changed during a bath addition (Figure 5.9).

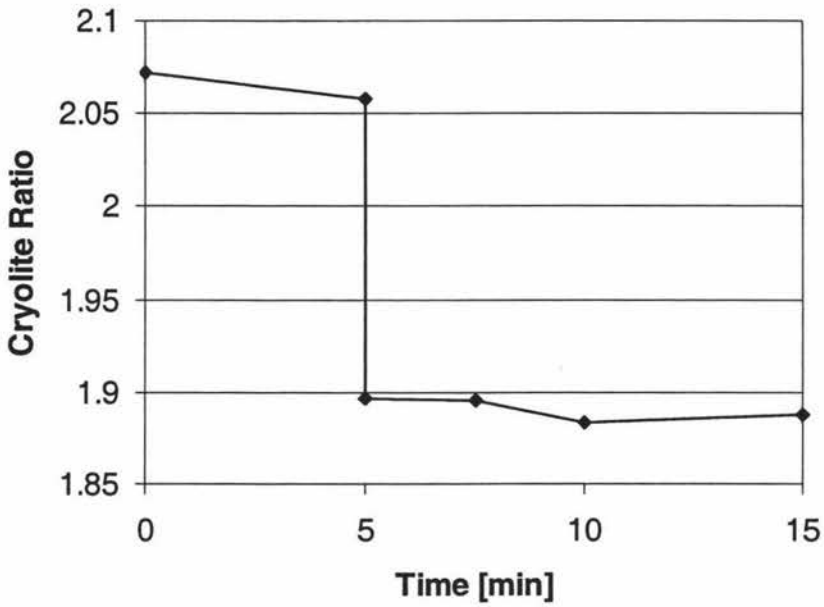

Figure 5.9 Cryolite ratio change during AlF_3 addition. AlF_3 addition at 5 minutes

Initially the measured cryolite ratio of the electrolyte was approximately 2.05, corresponding well with the weighed in cryolite ratio of 2.0. At 5 minutes, AlF_3 was added to the bath, and is shown to immediately change the cryolite ratio measured from the bath samples. The measured cryolite ratio after the AlF_3 addition was 1.88, which is very close to the calculated cryolite ratio of 1.85. This shows that the bath mixing quickly distributes the added AlF_3 throughout the bulk of the bath. This analysis however, does not show whether the added AlF_3 has dissolved and effected the activities of the electrolyte. X-ray diffraction may be more useful in this regard, as any AlF_3 present as a particulate rather than a dissolved species (which will be solidified as chiolite) will be identifiable.

Experiments using the closed tube design electrodes to measure the potential changes from cryolite ratio changes were also carried out. The change in the measured potential for both additions of AlF_3 and cryolite were examined (Figure 5.10)

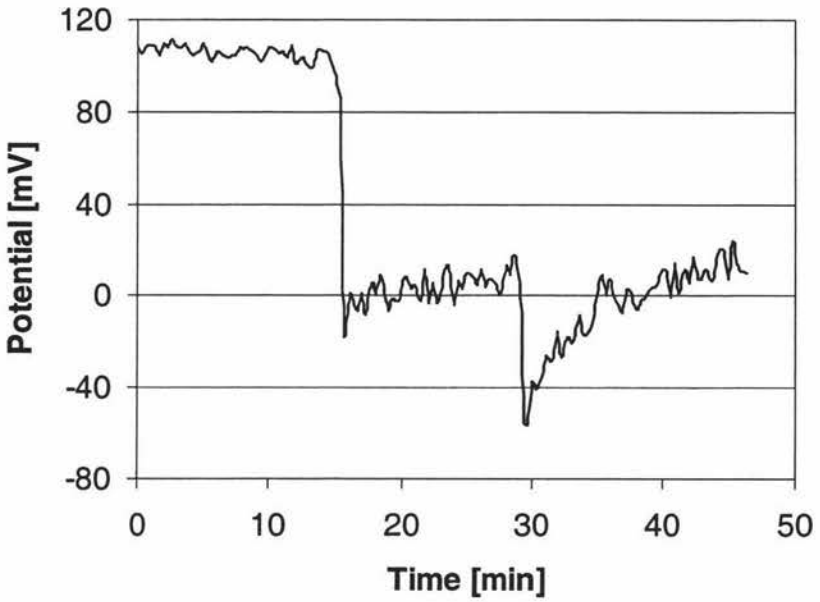

Figure 5.10 Potential vs. Time – Closed Tube Design, T=1000°C, CR 1.6-1.4 at 15min, CR 1.4-1.5 at 28min.

The calculated potential step of –76 mV for changing the cryolite ratio from 1.6 to 1.4 is quite close to the experimental value of –95 mV. Furthermore, the addition of cryolite, to increase the cryolite ratio from 1.4 to 1.5 results in an observed potential change of approximately 20 mV, which although is a factor of 2 different from the theoretical change of 41 mV, is in the correct direction. Like AlF_3, additions of cryolite may not immediately change the cryolite ratio of the bulk bath. During the dissolution of any added cryolite, the liquidus temperature of the electrolyte increases. This combined with the drop in bath temperature due to the cryolite addition, means that the superheat of the bath decreases quickly, increasing the likelihood of the electrolyte freezing. This frozen electrolyte then must dissolve before the cryolite ratio of the bath reaches the desired target.

Several attempts were made to examine the potential changes from AlF_3 additions at higher cryolite ratios. However the noise in the potential measurements were often too large for any clear potential steps to be observed. The problems due to bath freezing will be increased at higher cryolite ratios, as the available superheat is less, and therefore more freezing will occur.

5.1.5 Absolute Potentiometric Measurement of the Cryolite Ratio

To remove any problems associated with changing the cryolite ratio during experiments (i.e. inadequate mixing, bath freezing), attempts were made to measure the absolute potential between two electrodes, and correlate this to the cryolite ratio of the electrolyte. The results obtained over several experiments, with fresh close tube electrodes used for each experiment, were plotted over time (Figure 5.11).

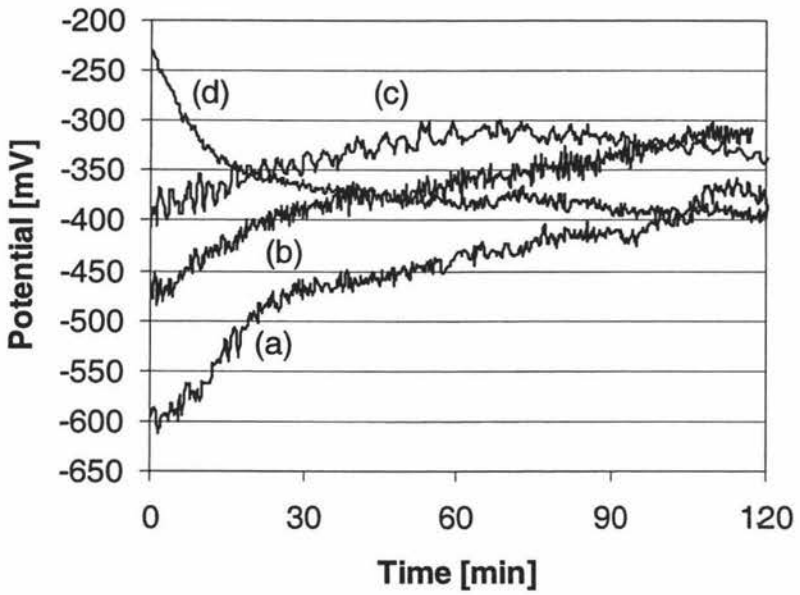

Figure 5.11 Potential vs. Time at various Cryolite Ratios – (a) CR=1.2, (b) CR=1.6, (c) CR=2.0, (d) CR=2.8 T=1000°C

The results for cryolite ratios of 1.2, 1.6 and 2 are consistent with the thermodynamic data, in that the absolute potentials are lower at lower cryolite ratios over the experimental period. This trend is not continued when the potential was measured in a electrolyte with a cryolite ratio of 2.8. This could be explained by unexpected changes in the electrode's activity, especially the activity of sodium in the sodium alloy electrode. The activity of the sodium in the sodium alloy was assumed to be equal at the start of each experiment. This may not be the case, especially if the Pb-Na alloy was not completely homogenous in composition during the casting of the small rods of alloy. Activity changes in the rods during storage is considered to be negligible as the alloy

was keep in dry air tight vessels, to reduce any oxidation reactions. It is more likely that the activity of sodium within the Pb-Na electrode changed during the experiments. This is examined later in section 5.1.8.

If the activity of sodium is changing during the experiments, then it could be beneficial examining the initial potential measurements before any significant activity changes could occur. The initial potentials measured between the electrodes are in the correct relationship to each other in respect to the cryolite ratio (Figure 5.11). The difference in the initial potentials (i.e. those at t = 0) can be compared to the theoretical differences (as in 5.1.3) arising from the change in electrolyte activities at the different cryolite ratios (Table 5.2).

Table 5.2 Comparison of Initial Potentials at Various Cryolite Ratios

Cryolite Ratio Change	Theoretical Potential Difference [mV]	Observed Potential Difference [mV]
1.2-1.6	195	125
1.6-2.0	108	75
2.0-2.8	130	175

The observed potential differences arising from the different electrolyte compositions are not identical but are of a similar magnitude to the theoretical differences calculated from the thermodynamic data. This variance between the observed and theoretical potential differences would most likely arise from a combination of factors such as bath temperature changes, electrolyte freezing, heterogeneous bath composition, and sodium activity changes. This work shows that the initial potential readings might actually be more useful in determining the cryolite ratio, than potential readings taken after the electrodes have been in the electrolyte for some time. The activity of the sodium electrode may change quite quickly once immersed into the molten electrolyte and measurements made after some time will have errors because of this.

It is suggested that further work should examine the use of initial potential readings for cryolite ratio measurement rather than "stabilised" potentials recorded after some time. This may involve the development of new electrodes, which have a different configuration more suitable to quick measurements. Electrodes with a lower thermal mass would be beneficial, as less freezing would occur during the immersion of the electrode into the molten electrolyte. It is suggested that such electrodes could be developed as single use sensors, eliminating the effect of changes in the electrode's activity. One suggested design is shown, with the concept based on a hanging drop electrode (Figure 5.12).

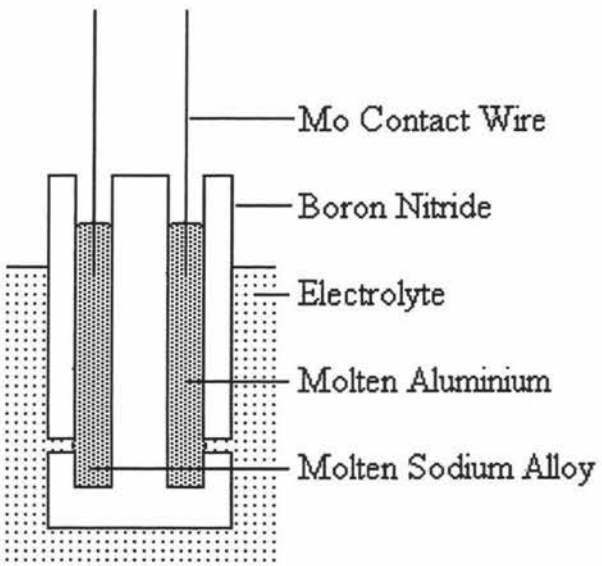

Figure 5.12 Suggested Future Electrode Design

This design combines both the sodium alloy and aluminium electrode into one body, which reduces the overall thermal mass of the sensor by around half. The design has two electrode reservoirs that hold the molten sodium alloy and aluminium. The reservoirs are open to the molten electrolyte via small holes situated near the bottom of the reservoir. Provided that the hole is small enough, the molten metal should not leak from the hole, but provide a positive pressure inhibiting the intrusion of electrolyte into the electrode body. This design is similar to the hanging drop electrode, where a drop of mercury is hung from a fine capillary, but not allowed to drop.

5.1.6 Stability and Accuracy of Static Electrode Designs

The stability of electrodes used for potentiometric measurements is important for reliable and reproducible potential measurements to be made. Small drifts in an electrode's activity may be acceptable provided that this drift is easily accounted for in the calibration or measurement technique. Typically workers using cryolite-based melts suggest that the stability of around ± 5 mV is normally acceptable [43,48]. As the electrode system is designed principally for cryolite ratio or cryolite ratio change measurement, the magnitude of the measured potential upon cryolite ratio changes must be larger than the error associated with the measured potential in order for any cryolite ratio changes to be detectable. Paragraph 5.1.3 discusses these theoretical potential changes, and, as mentioned, the electrode arrangement should be sensitive enough to detect potential changes of at least 11.6 mV.

Early results using both electrode designs showed that reproducible results could not be achieved on a regular basis. Typically most experimental results showed a minimum error or noise of ± 10 mV which would prevent small changes in the cryolite ratio being detected. Furthermore the potentials measured by the static electrode arrangements was often far too unstable for any conclusions to be made regarding the electrolytes composition. Often the potential measurements would either drift by up to ± 50 mV per hour or show large step changes, not corresponding to any apparent composition or operating condition change. This instability may be caused by either electrode damage, changes in electrode activity, uncontrollable electrolyte changes, or external electrical interference.

5.1.7 Electrode Damage and Construction Analysis

Electrode damage often occurred after several hours of use in the cryolite-based baths. The most obvious sign of electrode damage was the cracking of the boron nitride body, which was observed much more frequently in the aluminium electrode. This is consistent with literature concerning the corrosion of boron nitride in cryolite melts [63], where the rate of corrosion is increased in the presence of aluminium. This may be due to the formation of aluminium nitride [63]. Scanning electrode microscope (SEM) photographs showed that an interface layer is formed between the liquid aluminium and the boron nitride body of the aluminium electrode (Figure 5.13). This interface layer may not only be damaging to the electrode body, but also effect the contact between the electrolyte and the liquid aluminium. This may be another possible cause for the observed drift in the measured potential during many experiments. There is a noticeable structure difference between the interfacial layer (Figure 5.13) and the fresh boron nitride (Figure 5.4a) and boron nitride that has been immersed in molten electrolyte (Figure 5.4b). The particles which make up this layer appear to be more disordered and this layer also has small amounts of what appears to be frozen electrolyte, which would have infiltrated through the pores of the boron nitride. Using non-porous pyrolytic boron nitride would reduced the observed damage however this would mean that the closed tube design, which utilises the porosity of the hot pressed boron nitride, would need to be redesigned.

During several experiments, large steps in the measured potential were observed. On further inspection it was seen that the liquid aluminium pool did not wet the boron nitride body of the electrode. An oxide layer on the aluminium is believed to cause this non-wetting of the boron nitride. This oxide layer causes the aluminium to "ball up" and any movement of the electrode changes both the electrolyte-aluminium and the aluminium-molybdenum wire contact. By alloying the aluminium with a metal such as tin, this non-wetting was avoided and the large steps in the potential measurements caused by electrode movement reduced. Later experiments used a Sn-Al alloy (25 wt% Al) in the aluminium electrode which improved the overall stability and noise as shown by Figure 5.14.

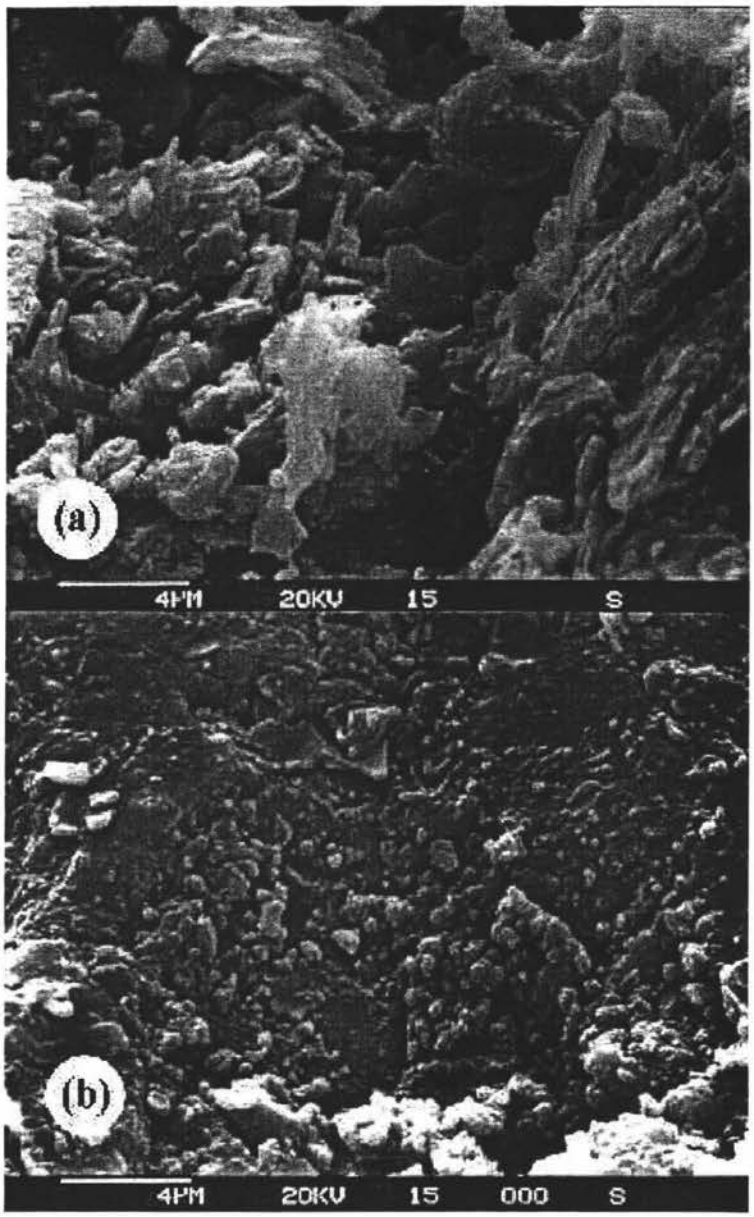

Figure 5.13 SEM Photographs of Boron Nitride - Aluminium interface layer (a) Al side (b) BN side.

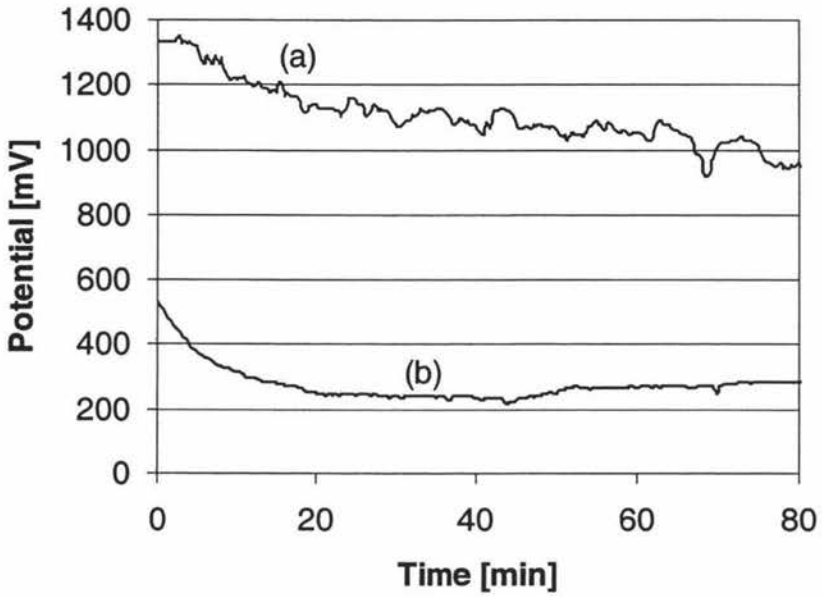

Figure 5.14 Potential vs Time – Closed Static design (a) Al / Pb-Na, (b) Sn-Al / Pb-Na

The difference in the absolute potentials measured between the two electrode arrangements arises from the difference in the aluminium activity of the two aluminium electrodes (see Equation 1.16).

5.1.8 Changes in the Sodium Activity

Changes in an electrodes activity, especially the sodium activity, has been discussed as a cause for the observed instability of potential measurements between a sodium alloy electrode and an aluminium electrode [3]. In this work the Pb-Na alloy was analysed after several experiments to determine any sodium loss and its possible effect on the measured potential. Equation 1.16 shows that a reduction in the sodium activity would cause a net decrease in the absolute measured potential. The activity of sodium in lead alloys follows a logarithmic relationship over the concentration range of 0.157 to 0.572 sodium mole fraction [64].

Atomic absorption spectroscopy was used to measure any change of the sodium concentration in the Pb-Na electrode metal. The results showed that the sodium

concentration decreased from 4.95 mole % to between 2.11 and 2.49 mole %, after the electrodes were emerged in the molten electrolyte for 2 hours. The cryolite ratio of the electrolyte did not appear to influence the loss of sodium from the Pb-Na alloy.

It is suggested that the change in the sodium concentration of the Pb-Na alloy be further investigated, in particular the rate at which this change occurs. This information could be used in estimating the maximum working lifetime of these electrodes before significant activity change occurs.

5.2 Bath Stability

Although electrode damage and experimental errors such as inadequate mixing can explain the apparent instability of the electrode system, it is also important to check the stability of the cryolite bath itself. An unstable measurement will arise from measuring an unstable bath composition.

5.2.1 Evaporation of Electrolyte

It is well known that the evaporation of electrolyte is a major factor in fluoride loss from aluminium smelters. The principal volatile species is $NaAlF_4$ [27], which has a cryolite ratio of 1. This shows that for the compositions examined in this work, there will be a net increase in the cryolite ratio as this species is lost. The vapour pressure over the NaF-AlF_3 system is shown to decrease with increasing cryolite ratio and decreasing temperature [27], indicating that the rate of evaporation is higher for melts with a lower cryolite ratio.

During most experiments the evaporation of electrolyte was highly evident by the build up of solids on the furnace lid. Some of this evaporated electrolyte was collected during several experiments and analysed by X-ray diffraction and the fluoride selective electrode method. The fluoride selective method indicated that the effective cryolite ratio was between 1.1 and 1.2. Pure $NaAlF_4$ has a cryolite ratio of 1, so this result indicates that other compounds also must be present. The diffraction pattern for this

evaporated species is shown in the Appendix. The pattern has peaks, which correspond to the pattern for $NaAlF_4$ [65], and also shows some peaks consistent with chiolite. The presence of chiolite is consistent with the results obtained from the fluoride selective electrode method. Ginsberg and Resch [66] suggested that NaF vapour reacts with the $NaAlF_4$ vapour to form chiolite. This could explain the chiolite peaks seen in the X-ray diffraction pattern.

The mass of the electrolyte was measured before and after every experiment, and used to determine the rate of evaporation. It should be noted that the evaporated rate calculated is the average rate taken over 2 hours, with the actual evaporation rate changing continuously during experiments as the cryolite ratio changes due to the evaporation. The results averaged over a number of experiments are shown in Table 5.3.

Table 5.3 Evaporation Rate from Cryolite Baths

Cryolite Ratio	Evaporation Rate [g/hr]	New Cryolite Ratio
1.2	24.7	1.23
1.6	20.4	1.69
2.0	12.6	2.09
2.4	8.8	2.5
2.8	6.5	2.9

The results obtained from these mass changes experiments are consistent with the vapour pressure data, with the evaporation rate increasing at lower cryolite ratios. Although the evaporation rate is significantly higher at lower cryolite ratios, because of the composition of the evaporated electrolyte, this does not mean that the rate of cryolite ratio change is higher also. Table 5.3 also shows the new cryolite ratio, calculated from the evaporation rate data (assuming CR=1 for evaporated electrolyte), after the electrolyte has been held at 1000 °C for 2 hours. The new cryolite ratio was confirmed

using the fluoride selective electrode method, with the results showing very similar changes in the cryolite ratio over 2 hours.

5.2.2 Freezing

Composition changes due to bath freezing are a common issue in industrial smelters when the delicate heat balance is upset [2,7]. When the freezing occurs at the side ledge of an industrial bath, cryolite is preferentially solidified into the ledge, changing the cryolite ratio of the remaining molten electrolyte. It is unclear if temperature changes in laboratory Hall-Héroult cells can result in composition changes due to electrolyte freezing. When sampling the cryolite bath using the inconel rod method, the rapid freezing results in a frozen sample, which reflects the bulk composition of the bath. This indicates that there is no preferential freezing of cryolite during this rapid quenching method. However additions of electrolyte, which cool the bath, may not cause such a rapid homogenous freezing of the electrolyte, especially if slower freezing occurs at some distance from the point of addition.

5.2.3 Mixing

Mixing of the cryolite bath is very important to ensure that the bath has a homogenous composition. As discussed in chapter 1 the bath's composition can affect many variables such as the liquidus temperature, which could lead to localised freezing if not kept even across the melt. Mixing is particularly important during electrolyte additions, when it is necessary to have fast dissolution of the added electrolyte, and a rapid change in the overall bath composition. Figure 5.15 shows how mixing effects the measured potential between two closed tube design electrodes. During this experiment the bath was mixed at a stirrer speed of 800 rpm.

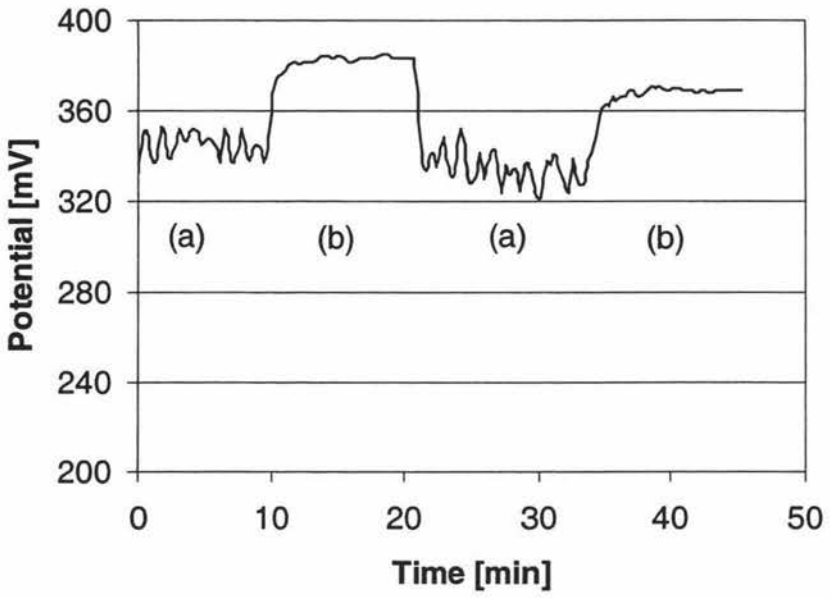

Figure 5.15 Effect of Bath Mixing on the Measured Potential
(a) Mixing at 800 rpm, (b) No Mixing

It is clear that during the periods of no stirring the measured potential has much less noise associated with it. The average potential is also seen to be around 40 mV higher during the unmixed stages. One explanation for the observed noise during mixing is that the mixing is not sufficient to maintain a homogenous composition. This could result in small variations in the composition "seen" by the electrode, as the bath is stirred. The disturbance in the contact between the electrodes and the electrolyte is another possible source of noise introduced by the stirrer. As previously discussed, the non-wetting of the boron nitride body by the aluminium electrode metal was improved by alloying the aluminium with tin.

Electrical noise could also arise when using the stirrer. An oscilloscope was employed in an attempt to detect signs of electrical noise. During early experiments some electrical noise was observed with a frequency of around 32 kHz. This was determined to be from the computer monitor used in the recording of the potentials. This noise was removed by careful location of the monitor and wires connecting to the electrodes.

5.3 Dropping Metal Electrode Flow Rate

An important aspect of dropping metal electrodes is obviously the flow rate of the liquid metal from the electrode. This is important in respect to both the metal-electrolyte interface and the available operating time of the electrode. This work looked at using liquid Pb-Na alloy as the dropping metal.

The first design based on the machined boron nitride tip gave results that indicate that this design is unsuitable due to the limitations imposed by machining capabilities. The typical flow rate was between approximately 130 and 430 mg/sec, which is an order of magnitude higher than the design flow rate of 40-65 mg/sec.

Table 5.4 Measured and Predicted Mass Flow rates (BN Tip)

Capillary Radius [mm]	Measured Mass Flow Rate [mg/sec]	Predicted Mass Flow Rate [mg/sec]
0.1	130	1580
0.15	430	8000

Capillary length = 3 mm, Pressure head = 8 cm

The measured flow rate was found to be considerably lower than the flow rate predicted by the Hagen-Poiseuille equation (Table 5.4). It is believed this is due to changes in the capillary during the experiment. As boron nitride is a relatively brittle material, small pieces of boron nitride often flake off throughout its use. This may cause blockages within the capillary inhibiting the flow rate of the molten metal. This was often observed with the flow rate stopping during many experiments.

The observed flow rates using the quartz capillary design showed more similarity to the calculated flow rates. The flow rate of mercury from the capillary was plotted as a function of the pressure head of mercury (Figure 5.16).

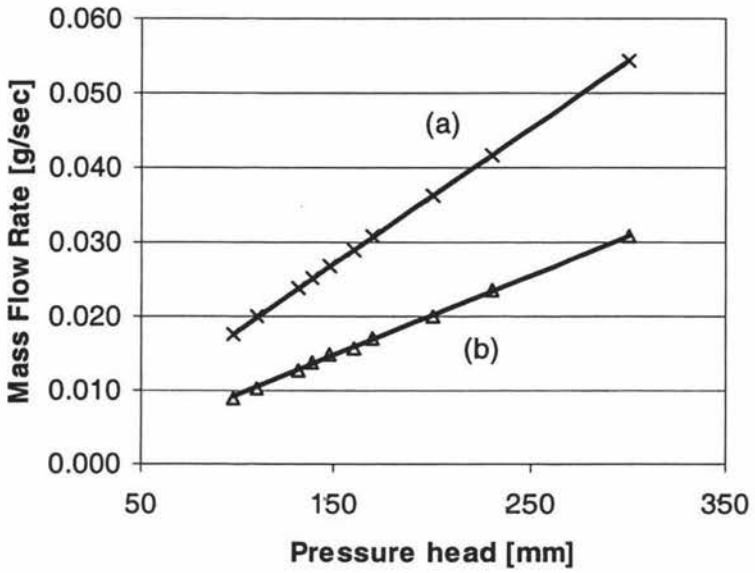

Figure 5.16 Mass Flow Rate from Quartz Capillary (a) Calculated (b) Measured

The difference between the calculated (using the Hagen-Poiseuille equation) and the observed flow rates most likely arose from a small contraction of the quartz capillary where the capillary was joined to the reservoir.

5.4 Potential Measurements using Dropping Electrode

Potential measurements between a dropping Pb-Na electrode and an Al-Sn closed tube electrode were carried out. Only the quartz capillary design was used here as the boron nitride tip design had mass flow rates too high for experiments of suitable length to be carried out. The flow rate of Pb-Na from the capillary was estimated to be an average of 5 mg/sec throughout the experiments. The results from an experiment carried out (CR=2.0, T=1000°C) show that a steady potential can be established between these electrodes (Figure 5.17).

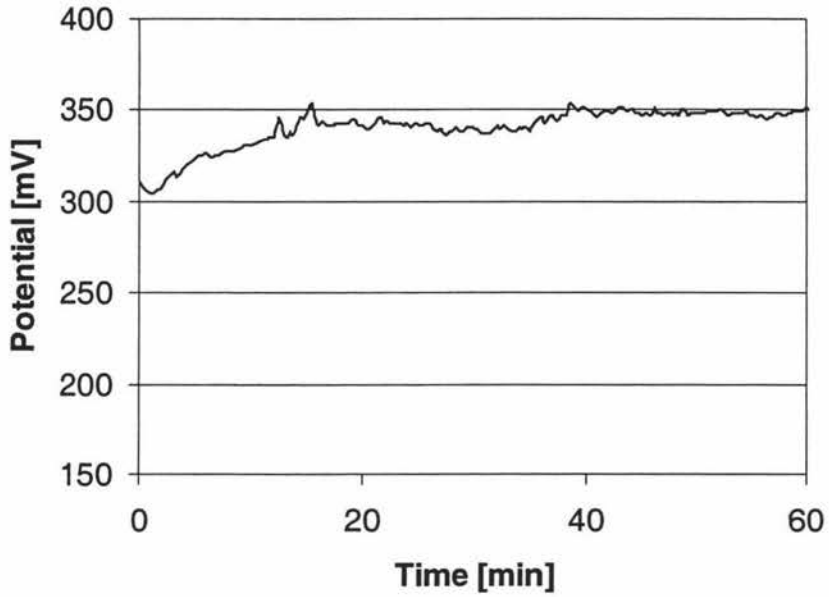

Figure 5.17 Potential vs. Time – Dropping Pb-Na Electrode

The potential between a closed static aluminium electrode and the dropping Pb-Na electrode was also measured during an addition of AlF_3 to the bath (Figure 5.18).

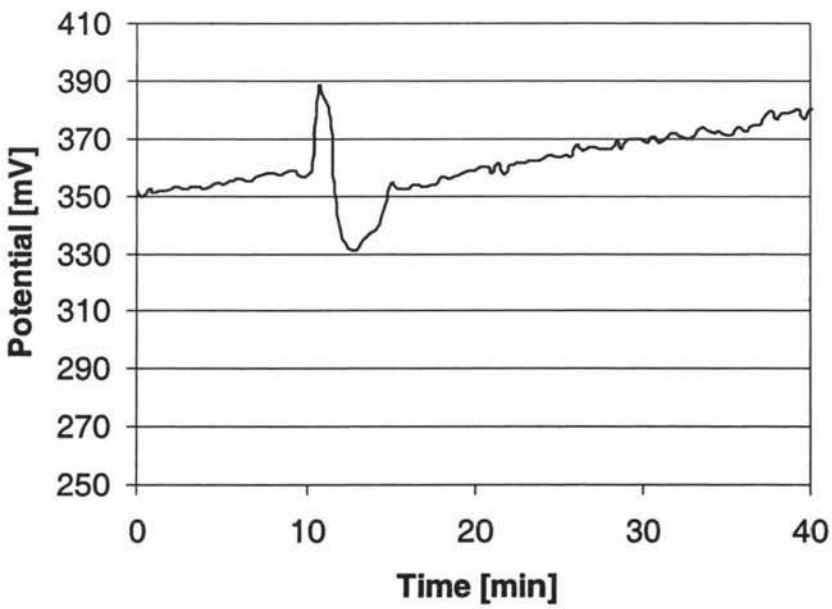

Figure 5.18 Potential vs. Time – Dropping Pb-Na Electrode, CR 1.9-1.75 at 10 minutes

The potential is seen to initially increase before a decrease of approximately 25 mV from the stable potential is measured. This drop in potential is consistent with the theoretical decrease of 40 mV, however the potential soon increases back past the initial stable potential. This gradual increase is thought to be due to a failure of the dropping electrode. During this experiment the mass change of the dropping electrode was considerably less than expected from the typical mass flow rate observed from the electrode. This indicates that the flow rate may have stopped at some point during the experiment. This means that the main benefit of the continuously renewing electrode surface will be lost, and the electrode activity will change as sodium is dissolved into the electrolyte. It must be pointed out however, that activity changes in the sodium electrode should only effect the absolute potential and not the potential change resulting from an AlF_3 addition. This shows that the observed irregularities in the measured potential (Figure 5.18) must arise from a combination of effects such as electrode activity changes, electrolyte composition instability, electrolyte freezing, and mixing.

Overall the dropping electrode constructed around the quartz capillary, gave unsatisfactory results due to the very limited lifetime. This electrode was significantly damaged within 2 hours of use in the electrolyte environment. However the principle of this electrodes design (the continuously renewing electrode surface) appeared to give more stable potential measurements than the static electrode designs.

In respect to industrial application, it is felt that the construction and operation difficulties of this electrode rule it out as a part of an industrial sensor. Further work could be carried out to investigate the use of this electrode arrangement in other potentiometric applications such as activity measurements in molten salts where other electrodes prove to be unsuitable.

6 Conclusions and Recommendations

This work examined the potentiometric measurement of the cryolite ratio using two different basic electrode designs, the static pool electrode and the dropping electrode. The use of a dropping metal electrode for direct potentiometric analysis is believed to be a first, even though the electrode was developed almost one hundred years ago.

Potential measurements made during changes in the cryolite ratio corresponded to the predicted direction of potential change and were of similar magnitude to the theoretical potential changes calculated from activity data. This indicates that this method of cryolite ratio measurement shows a lot of promise and may lead to better control of electrolyte composition within industrial smelters. There was however some problems associated with the stability and reproducibility of the potential measurements. This is suggested to be due to damage to the electrodes and unexpected changes in the electrolyte composition during the experiments. Evaporation, bath freezing and inadequate mixing are suggested to cause these unexpected composition changes. The bath composition was shown to change by as much as 0.1 cryolite ratio units over a 2 hour experiment. This is mainly due to the evaporation of $NaAlF_4$, which was confirmed by X-ray diffraction as the principal species found in the solidified vapour.

Absolute potential measurements were also made between the electrodes and correlated against the cryolite ratio of the electrolyte. The results obtained with the static pool electrodes were again effected by changes in the bath composition and damage to the electrodes by the corrosive electrolyte. The instability of the bath composition meant that any potential measurements also reflected these changes making the overall stability of the measurement system hard to quantify. Activity changes in the static pool electrodes, especially in the sodium alloy electrode, also affected the absolute potential measurements. The sodium concentration in the Pb-Na alloy electrodes was shown to decrease from 4.95 mole % to between 2.11 and 2.49 mole % after these electrodes had been immersed in the molten electrolyte for 2 hours. The cryolite ratio of the electrolyte appeared to have no effect on the loss of sodium from the alloy.

To remove the effect of both bath composition and electrode activity changes during experiments, potential measurements were made immediately after the electrodes were placed in a range of electrolyte compositions. The differences in these initial potential readings were similar to the theoretical potential differences arising from the change in electrolyte composition. This further confirms the effect of electrode damage, electrolyte instability and electrode activity changes, which all become significant after the electrodes have been immersed in electrolyte for some time. It is suggested that these initial potential measurements may be more useful in respect with developing a commercial cryolite ratio sensor, and new single use electrodes should be developed to investigate this.

The electrode damage, which is believed to contribute to a lot of the error found in many of the potential measurements, was further investigated. Boron nitride corrosion and cracking was highly evident in all electrodes especially in the presence of aluminium. SEM photographs suggested that an interface layer is formed between the liquid electrode metal and the boron nitride body. Further development of the electrodes must be carried out to prevent damage caused by the high temperatures and corrosive electrolyte. Using non-porous pyrolytic boron nitride instead of hot pressed boron nitride may reduce the level of damage as electrolyte intrusion into the electrode material will be reduced.

Work carried out with dropping metal electrodes, showed that direct potential measurements could be made between a drop of electrode metal and another electrode. These measurements were observed to have less noise and a higher stability than the static pool electrodes that were investigated. This is in line with the renewing electrode surface that is characteristic of dropping electrodes. More work needs to be carried out to improve the working lifetime of these electrodes, as the high temperatures and corrosive electrolyte damaged the electrodes within several hours. Although dropping electrodes may not be very useful for industrial sensor or control applications, they may be of use in other molten salt environments where other electrodes tend to fail due the activity changes.

Overall the work shows that further development of electrodes for use in cryolite-based electrolytes needs to be carried out, before reliable potentiometric measurements of the cryolite ratio can be made.

Reference List

1. Plunket P.A., (2001) "Aluminium" U.S. Geological Survey, Mineral Commodity Summaries,

2. Utigrad T.A. (1999) "Why 'Best' Pots Operate between 955 and 970 °C" Light Metals, p 319-326.

3. Gudbrandsen H., Haarberg G.M., Olufsen F., and Rolseth S., (1998) "A Laboratory Probe for Bath Acidity of Cryolite-Alumina Melts" Light Metals, p 367-370.

4. Haupin W. E, (1987) "Chemical and Physical Properties of the Electrolyte" Production of Aluminium and Alumina, Burkin A.R. Ed, John Wiley & Sons, New York, p 85-87.

5. Dewing E.W., (1970) "Liquidus Curves for Aluminium Cell Electrolyte. V. Representation by Regression Equations" Journal of the Electrochemical Society, 117 p 780-781.

6. Holm J.L, (1973) "The Lattice Energy and Thermochemical Properties of the Compound $NaAlF_4$, Sodium Tetrafluoroaluminate" Acta Chemica Scandinavica, 27 p 1410-1416.

7. Mann V.K., Yurkov V.V., Polyakov P.V., and Buzunov V.Y. (1998) "Cryolite Ratio and Bath Temperature Stabilization Problem in Aluminium Reduction Cell" Light Metals, p 371-377.

8. Rolseth S., Verstreken P., and Kobbeltvedt O., (1998) "Liquidus Temperature Determination in Molten Salts" Light Metals, p 359-366.

9. Haupin W., (1992) "The Liquidus Enigma" Light Metals, p 447-480.

10. Wang X., Peterson R.D., and Tabereaux A.T., (1992) "Electrical Conductivity of Cryolite Melts" Light Metals, p 481-448.

11. Utigrad T.A., (1993) "Density of the Na_3AlF_6-AlF_3-Al_2O_3-CaF_2 System: A Key to the Performance of the Hall-Héroult Cells" Light Metals, p 239-245.

12. Gerlach J. and Winkhaus G., (1985) "Interaction of Alumina with Cryolite-Based Melts" Light Metals, p 301-313.

13. Gerlach J., Hennig U., and Hern K., (1975) "The Dissolution of Aluminium Oxide in Cryolite Melts" Metallurgical Transactions, 6B p 83-86.

14. Stevens F.J., Zhang W., Taylor M.P., and Chen J.J.J., (1992) "The Interaction between Current Efficiency and Energy Balance in Aluminium Reduction Cells" Light Metals, p 541-547.

15. Tarcy G.P. and Sorensen J., (1991) "Determination of Factors Affecting Current Efficiency in Commercial Hall Cells using Controlled Potential Coulometry and Statistical Experiments" Light Metals, p 453.

16. Foster P.A., (1975) "Phase Diagram of a Portion of the System Sodium Hexafluroaluminate-Aluminium Fluoride-Aluminium Oxide" The Journal of the American Ceramic Society, 58 (7-8), p 288-291.

17. Haverkamp R.G., (2000) "Removal of the Anode Effect" Aluminium Transactions, 2 (1), p 169-174.

18. Yoshida K. and Dewing E.W., (1972) "Apparent Solubility of Aluminium in Cryolite Melts" Metallurgical Transactions, 3 (7), p 1817-1821.

19. Grjotheim K. and Welch B.J., (1988) "Bath Chemistry - The Electrolyte" Aluminium Smelter Technology , 2nd Edition, Aluminium-Verlag, Düsseldorf, Germany p 64.

20. Grjotheim K., Krohn C., Malinovský M., Matiašovský K., and Thonstad J., (1982) "Physical-chemical Properties" Aluminium Electrolysis, 2nd Edition, Aluminium-Verlag, Düsseldorf, Germany, p 152-167.

21. Choudhary G., (1973) "Electrical Conductivity for the Electrolytes of Aluminium Extraction Cell" Journal of Electrochemical Society, 120 (3), p 381.

22. Wang X., Peterson R.D., and Tabereaux A.T., (1993) "A Multiple Regression Equation for the Electrical Conductivity of Cryolite Melts" Light Metals, p 247-255.

23. Paucirova M., Matiašovský K., and Malinovský M., (1970) "Volume Properties of the Melts of the Systems LiF-AlF_3 and NaF-AlF_3" Revue Roumaine de Chimie, 15 p 33-41.

24. El-Demerdash M.F., Khalil E.E., El-Raghy S.M., and Moustafa F.A., (1998) "Estimation of Cell Efficiency Based on the Rate of Aluminium Transfer to Anode" Light Metals, p 491.

25. Vassiliadou V., Paspaliaris I., Stefanidis D., and Georgantonis D., (1993) "Energy Savings in Aluminium Electrolysis by Continual Monitoring and Control of the AlF_3 Content of the Cryolitic Melt" Energy Efficiency in Process Technology, Pilavachi P.A. Ed., Elsevier Applied Science, London and New York, p 1181-1190.

26. Stevens McFadden F.J., Welch B.J., Whitfield D., and Skyllas-Kazacos M., (2001) "Control of Temperature in Aluminium Reduction Cells Challenges in Measurements and Variability" Light Metals, p 1171-1178.

27. Grjotheim K., Kvande H., Motzfeldt K., and Welch B.J., (1972) "The Formation and Composition of the Fluoride Emissions from Aluminium Cells" Canadian Metallurgical Quarterly, 11 (4), p 585-599.

28. Entner P.M., (1992) "Control of AlF_3 Concentration" Light Metals, p 369-374.

29. Rye K.A., Solberg I., Eidet T., and Rolseth S., (2001) "Aluminium Fluoride Dissolution and Distribution An Investigation of the Dynamic Mass Balance when Adding Large Quantities to a Prebake Cell" Light Metals, p 529-533.

30. Qui Z., Grjotheim K., Kvande H., Zhang J., and Sun T., (1993) "Influences of Additives on the Cryolite Ratio of Aluminium Electrolyte" Light Metals, p 291-296.

31. Baggio S. and Olavarria L.G., (1977) "Experimental comparison of some methods

for determining cryolite bath ratio in the alumina reduction process" Aluminium, 53 (12), p 737-740.

32. Grjotheim K. and Welch B.J., (1988) "Smelter Technology" Aluminium Smelter Technology , 2nd Edition, Aluminium-Verlag, Düsseldorf, Germany, p 253-261.

33. Jian F., Chongquig L., and Qiuwei W., (1993) "Determination of the Bath Ratio in Acid Aluminium Electrolyte by Flame AAS" Atomic Spectroscopy, 14 (5), p 154-156.

34. Topor D. and Birhala A., (1972) "Cryolite Bath Ratio by X-Ray Diffraction" Revue Roumaine de Chimie, 17 (6), p 961-968.

35. Crottaz O., Haverkamp R.G., Yellepeddi R., and de Nora V., (2001) "Development of Techniques for Measuring the Composition of Low Temperature Electrolytes" Light Metals, p 1195-1199.

36. Nagy K., Bjorgo R., and Fremstad D., (1984) "Routine Analysis of Bath Ratio: A New Method" Light Metals, p 501-512.

37. Wilson M.J., (1992) "Practical Considerations used in the Development of a Method for Calculating Aluminium Fluoride Additions Based on Cell Temperatures" Light Metals, p 375-378.

38. Desclaux P., (1987) "AlF_3 Additions Based on Bath Temperature" Light Metals, p 309-313.

39. Verstreken P.C., (2001) "Process for Controlling the AlF_3 content in Cryolite Melts" US Patent 6183620

40. Verstreken P. and Benninghoff S., (1996) "Bath and Liquidus Temperature Sensor for Molten Salts" Light Metals, p 437-444.

41. Haverkamp R.G. and Welch B.J., (2000) "Measurement of Alumina in Reduction Pots" US Patent 6010611

42. Bates C., (2001) "Method and Apparatus for Testing Material Utilizing Differential Temperature Measurements" US Patent 6220748

43. Grjotheim K., Krohn C., Malinovský M., Matiašovský K., and Thonstad J., (1982) "Electrochemical Properties" Aluminium Electrolysis, 2nd Edition, Aluminium-Verlag, Düsseldorf, Germany, p 194-207.

44. Sterten Å., Hamberg K., and Mæland I., (1982) "Activities and Phase Diagram of $NaF-AlF_3$ $-Al_2O_3$ Mixtures Derived from Electromotive Force and Cryoscopic Measurements. Standard Thermodynamic Data of $\beta-Al_2O_{3\,(s)}$ $Na_3AlF_{6\,(s)}$, $Na_5Al_3F_{14\,(s)}$ and $NaAlF_{4\,(l)}$" Acta Chemica Scandinavica, A, 36 p 329-344.

45. Sterten Å. and Mæland I., (1985) "Thermodynamics of molten Mixtures of Na_3AlF_6-Al_2O_3 and $NaF-AlF_3$" Acta Chemica Scandinavica, A, 39 p 241-257.

46. Solheim A. and Sterten Å., (1997) "Activity Data for the System $NaF-AlF_3$" Proceedings of the 9th International Symposium on Light Metals Production, Tromϕ - Trondheim, Norway August 18th - 21st p 225-234.

47. Solheim A. and Sterten Å., (1999) "Activity of Alumina in the system $NaF-AlF_3$-Al_2O_3 at NaF/AlF_3 molar ratios ranging from 1.4 to 3" Light Metals, p 445-452.

48. Burgman J.W., Leistra J.A., and Sides P.J., (1986) "A Reference Electrode for Hall Cell Experiments" Light Metals, p 463-472.

49. Sadoway D.R., (1988) "Aluminium Reference Electrode" US Patent 4764257

50. Kucera B., (1903) "For Surface Tension of Polarised Mercury" Annalen der Physik, 11 p 698-725.

51. Heyrovsky J., (1922) Chemicke-listy, 16 p 256-264.

52. Heyrovsky J. and Zuman P., (1968) "Principles of Polarography" Practical Polarography, Academic Press, London and NewYork

53. Hibbert D.B., (1993) Introduction to Electrochemistry, The Macmillan Press Ltd.

54. Laitinen H.A., (1967) "Polarography in Molten Salts" Pure and Applied Chemistry, 15 (2), p 227-237.

55. Heus R.J., Tidwell T., and Egan J.J., (1969) "Investigation of the Capacity of the

Electrical Double Layer in Molten Chlorides using a Dropping Electrode" Molten Salts, Symposium, p 499-508.

56. Naryshkin I.I., Yurkinskii V.P., and Yavich B.S., (1968) "Polarography in Molten Salts using a Dropping Lead Electrode" Khim. Khim. Tekhnol , 11 (1), p 23-26 .

57. Stehle G., Duruz J.J., and Landolt D., (1982) "High Temperature Polarography in Chloride Melts with Dropping Electrodes" Electrochimica Acta, 27 (6), p 783-789.

58. Hoff H., (1971) "Development and Operation of a Dropping Silver Electrode for Electrochemical Investigations on Molten Salts" Electrochimica Acta, 16 (7), p 1059-1069.

59. Heyrovsky J. and Kuta J., (1966) Principles of Polarography, Academic Press, New York and London.

60. Liu X., George S.F., and Wills V.A., (1994) "Visualization of Alumina Dissolution in Cryolitic Melts" Light Metals, p 359-364.

61. Weill D.F and Fyfe W.S, (1964) "The 1010° and 800°C Isothermal Sections in the System Na_3AlF_6-Al_2O_3-SiO_2" Journal of the Electrochemical Society, 111 (5), p 582-585.

62. Thornton G., (2001) Lenox Laser USA, Personal Communication.

63. Thonstad J., (1968) "Behaviour of Boron Nitride in Molten Cryolite and Aluminium" Electrochemical Technology, Abstract only 6 (9-10), p 346-349.

64. Chudakov I.P. and Marachevskii A.G., (1966) "Activity of Sodium in Lead Alloys at 660-1100 °K" Zh Prikl Khim, 39 (7), p 1647-1650.

65. Howard E.H., (1954) "Some Physical and Chemical Properties of a New Sodium Aluminium Fluoride" Journal of the American Chemical Society, 76 p 2041-2042.

66. Ginsberg H. and Resch K., (1960) "Structure of Salt Melts in the Systems NaF-AlF_3-Al_2O_3 under conditions of Aluminium Electrolysis" Erzmetall, 13 p 523-533.

Appendix

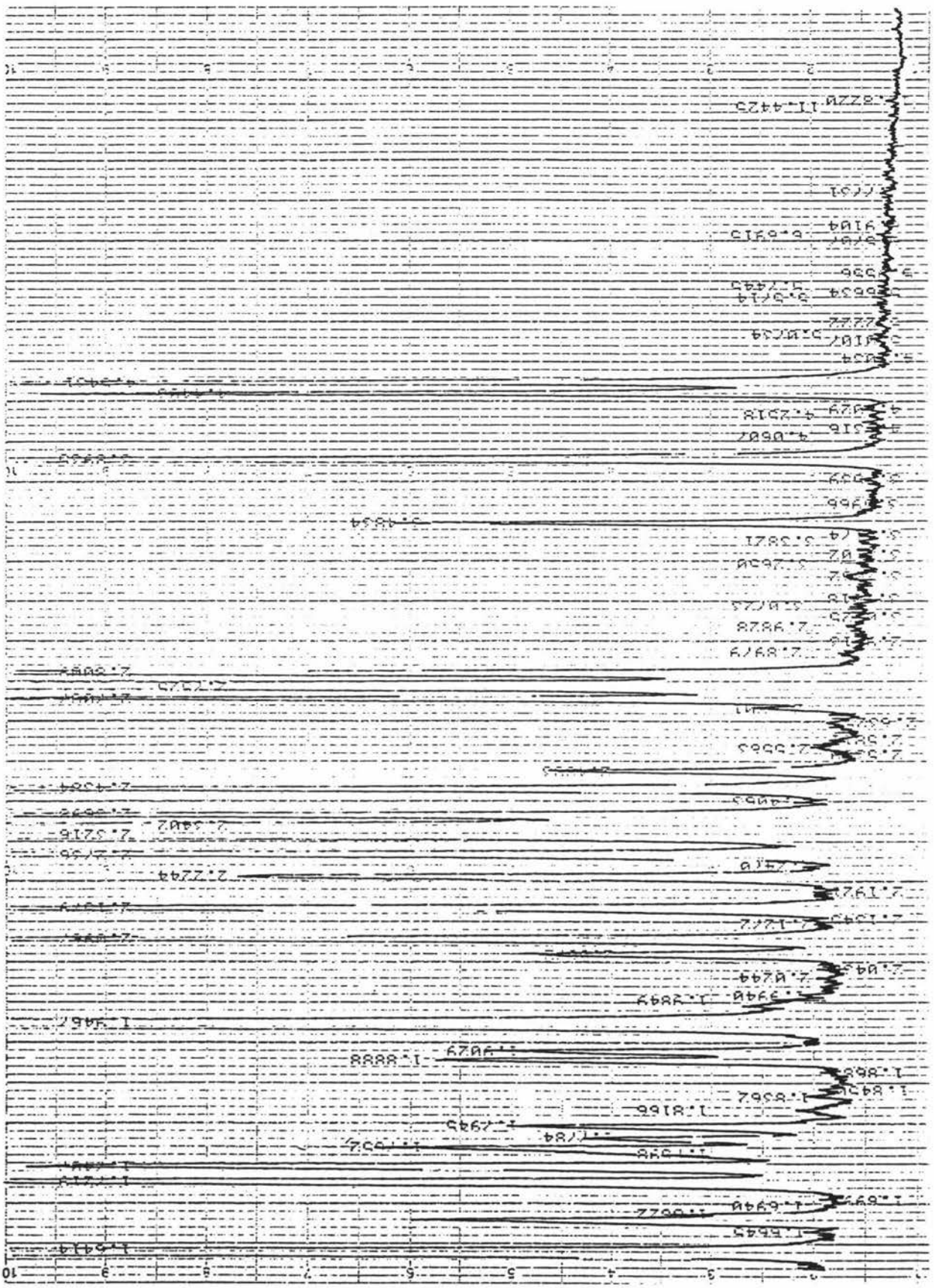

XRD Pattern - Sample (CR=1.6) + NaF Sinter

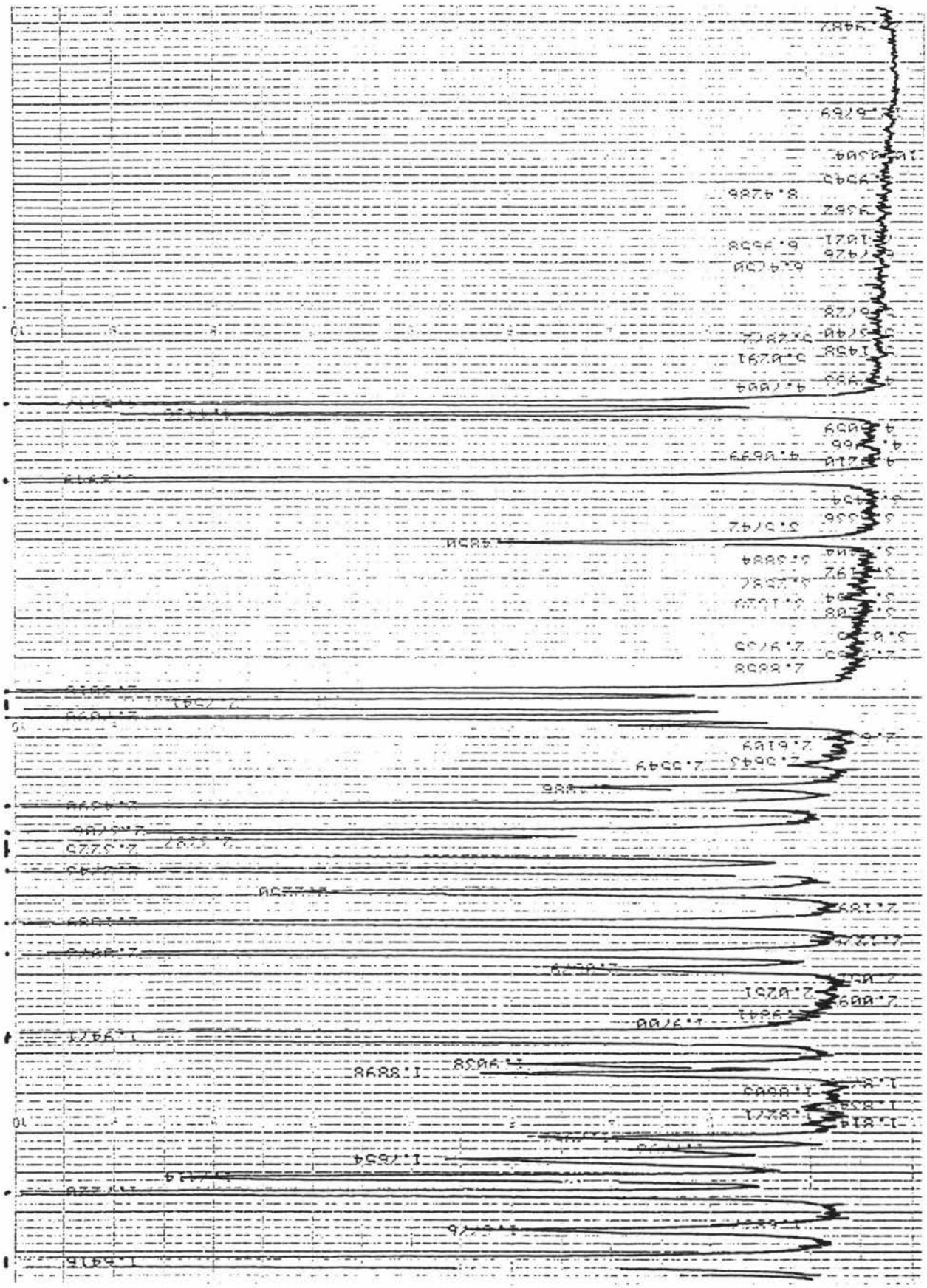

XRD Pattern - Sample (CR=2.4) + NaF Sinter

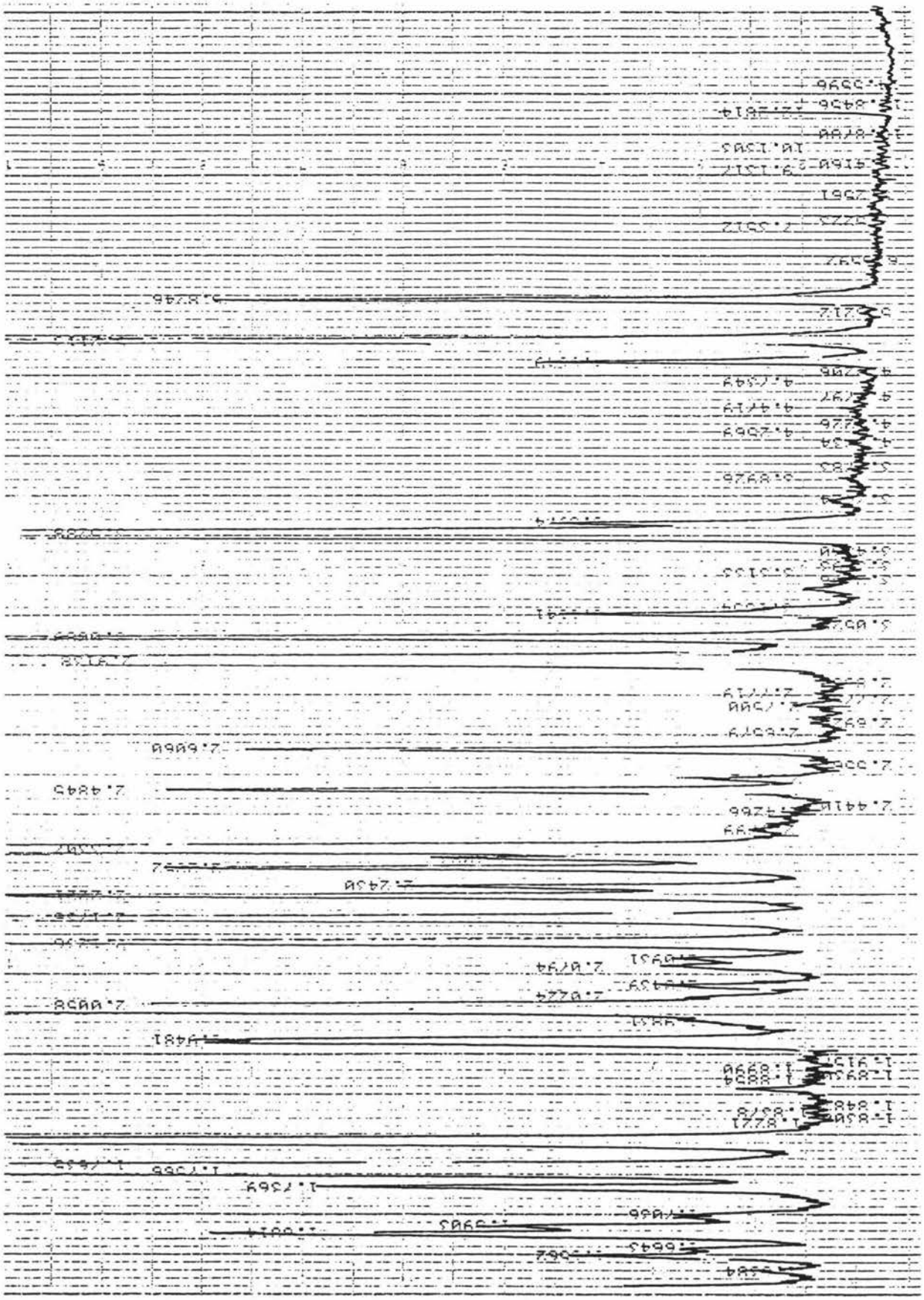

XRD Pattern - Sample CR=1.2

XRD Pattern - Sample CR=1.6

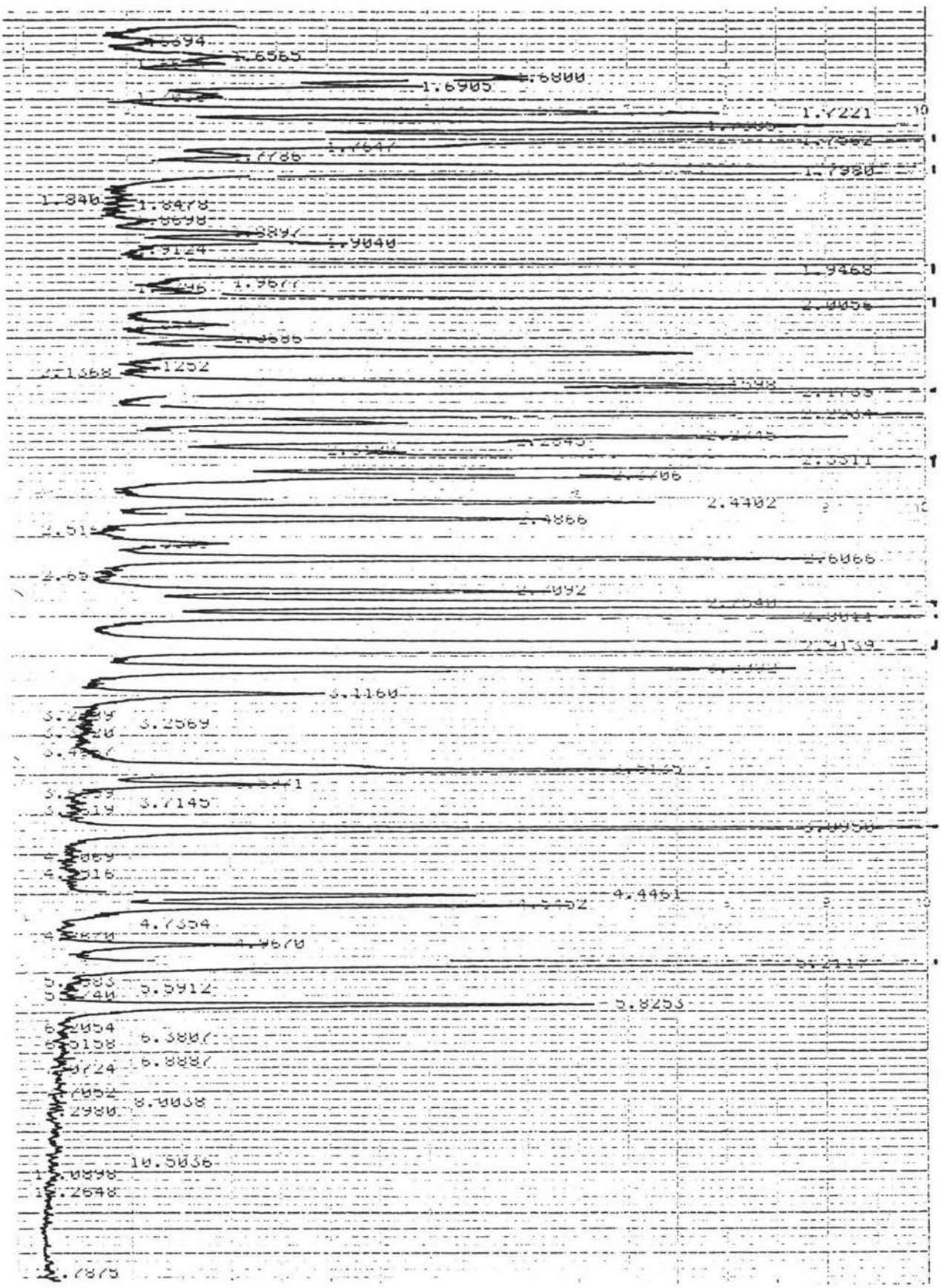

XRD Pattern - Sample CR=2.0

XRD Pattern - Sample CR=2.4

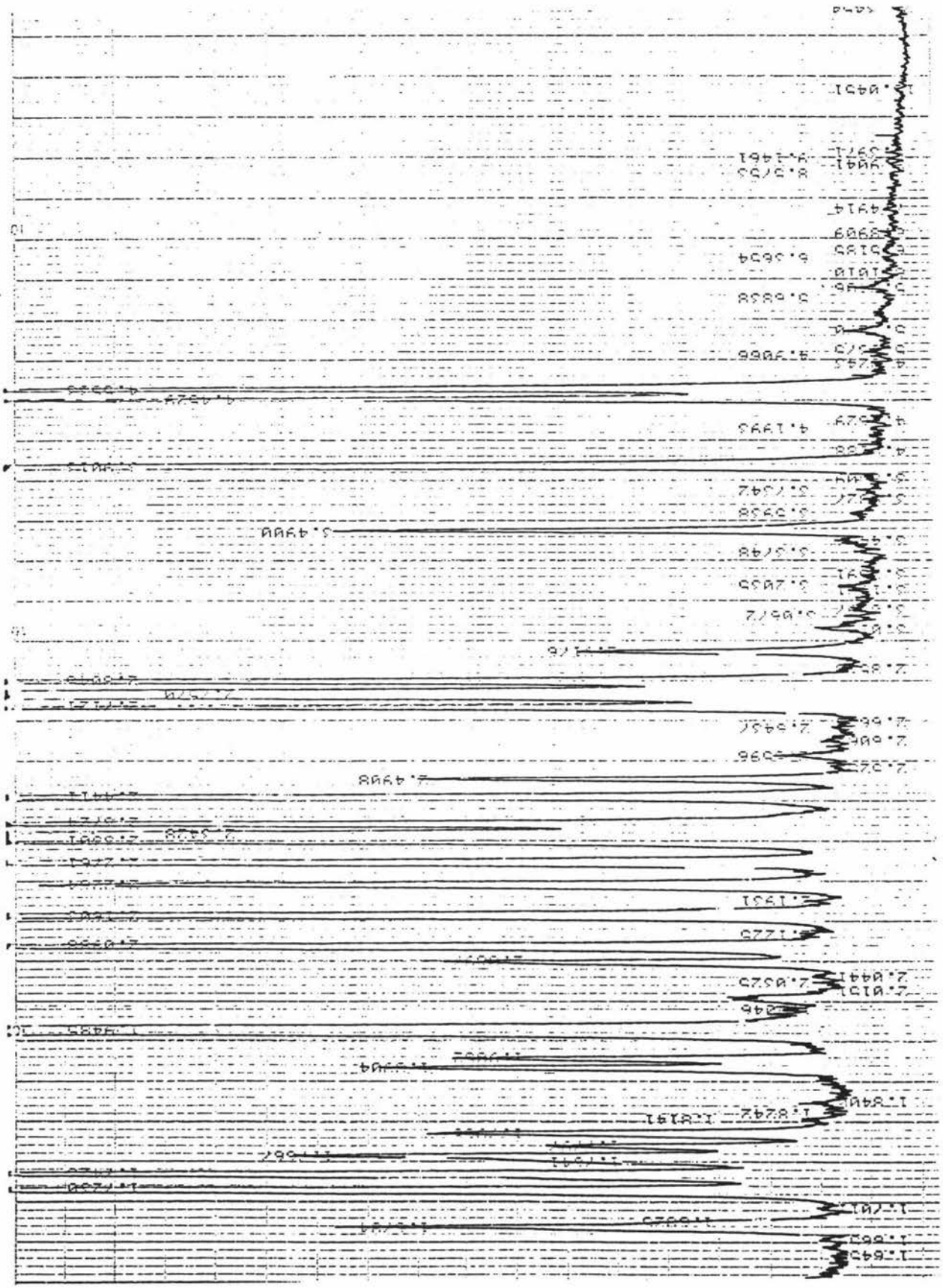

XRD Pattern - Sample CR=2.8

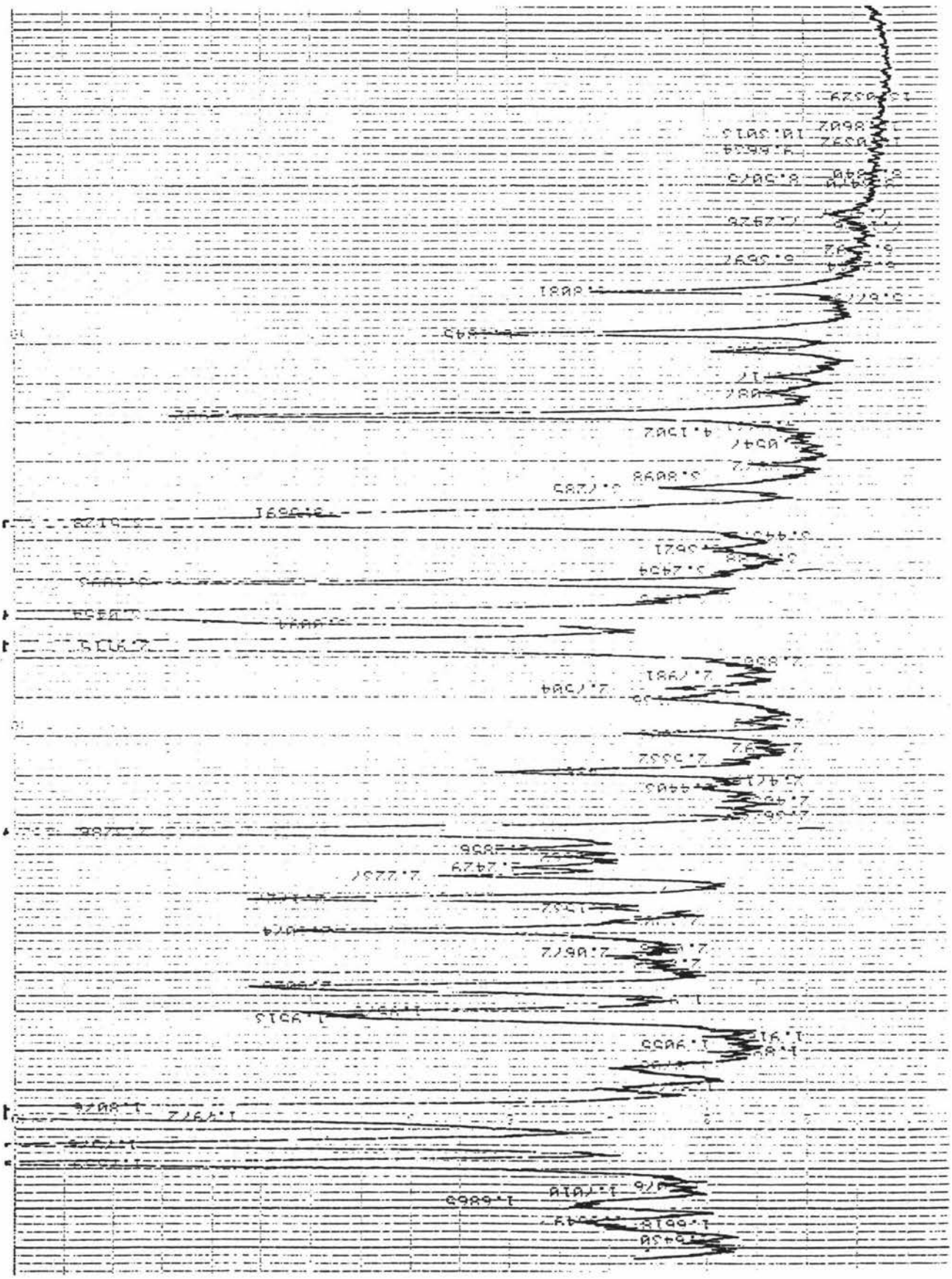

XRD Pattern – Evaporated Electrolyte